Engineering Radioprotective Human Cells Using the Tardigrade Damage Suppressor Protein, DSUP

Authors: Craig Westover[1], Deena Najjar[1], Cem Meydan[1], Kirill Grigorev[1], Mike T. Veling[3,4], Sonia Iosim[1], Rafael Colon[1], Sherry Yang[1], Uriel Restrepo[1] Christopher Chin[1], Daniel Butler[1], Chris Moszary[1], Savlatjaton Rahmatulloev[1], Ebrahim Afshinnekoo[1,2,5], Roger L Chang[3,4], Pamela A Silver[3,4], Christopher E. Mason[1,2,5,6]*

[1]Department of Physiology and Biophysics, Weill Cornell Medicine, New York, NY, USA
[2]The HRH Prince Alwaleed Bin Talal Bin Abdulaziz Alsaud Institute for Computational Biomedicine, Weill Cornell Medicine, New York, NY, USA
[3]Department of Systems Biology, Blavatnik Institute at Harvard Medical School, Boston, MA 02115, USA.
[4]Wyss Institute for Biologically Inspired Engineering, Harvard University, Boston, MA 02115, USA.
[5]The WorldQuant Initiative for Quantitative Prediction, Weill Cornell Medicine, New York, NY, USA
[6]The Feil Family Brain and Mind Research Institute, Weill Cornell Medicine, New York, NY, USA

*Corresponding Author
Christopher E. Mason
Weill Cornell Medicine
1305 York Ave., Y13-05
New York, NY 10021
Tel: 203-668-1448
E-mail: chm2042@med.cornell.edu

Abstract

Spaceflight has been documented to produce a number of detrimental effects to physiology and genomic stability, partly a result of Galactic Cosmic Radiation (GCR). In recent years, extensive research into extremotolerant organisms has begun to reveal how they survive harsh conditions, such as ionizing radiation. One such organism is the tardigrade (*Ramazzottius varieornatus*) which can survive up to 5kGy of ionizing radiation and also survive the vacuum of space. In addition to their extensive network of DNA damage and response mechanisms, the tardigrade also possesses a unique damage suppressor protein (Dsup) that co-localizes with chromatin in both tardigrade and transduced human cells and protects against damage from reactive oxygen species via ionizing radiation. While Dsup has been shown to confer human cells with radioresistance; much of the mechanism of how it does this in the context of human cells remains to be elucidated. In addition, there is no knowledge yet of how introduction of Dsup into human cells can perturb cellular networks and if there are any systemic risks associated. Here, we created a stable HEK293 cell line expressing Dsup via lentiviral transduction and confirmed its presence and its integration site. We show that Dsup confers human cells with a reduction of apoptotic signals. Through measuring these biomarkers of DNA damage in response to

irradiation longitudinally along with gene expression analysis, we were able to demonstrate a potential role for Dsup as DNA damage response and repair enhancer much in the same way its human homologous counterpart HMGN1 functions. Our methods and tools provide evidence that the effects of the Dsup protein can be potentially utilized to mitigate such damage during spaceflight.

Introduction

As more public and private enterprises plan to send humans on long-term spaceflight missions, the challenges associated with adapting to the harsh conditions of space become more pronounced. One of the major risks to humans during spaceflight is the exposure to Galactic Cosmic Rays (GCRs), which are made up of mostly high-energy protons, and to a lesser extent, alpha particles, electrons, and highly damaging HZE nuclei [1,2]. High linear energy transfer (LET) radiation in general produce more carcinogenic and complex breaks leading to genomic instability than low LET radiation[1]. Low LET radiation such as ϒ-rays and x-rays deposit their energy uniformly but still produce double stranded breaks mainly through the indirect method of increasing reactive oxygen species (ROS) through the radiolysis of water[1-4]. Low LET-induced oxidative stress is then defined as an imbalance between a lack of anti-oxidative defenses against an excess of ROS[5-7].

As of now there is little data on the associated risks of exposure to space radiation for a 3-year Mars mission[8], but it has been estimated that a return trip to Mars could expose astronauts to 600-1000mSv, which is near the NASA astronaut career limit of 800-1200mSv[1,2]. Based on these estimates, the predicted attributable risk for GCR exposure would suggest a high likelihood of returning astronauts facing higher risk of leukemia, stomach, colon, lung, bladder, ovarian, and esophageal cancers[2]. Selection of radioresistant individuals for space travel has been proposed as one option to circumvent the effects of these massive doses of radiation exposure. Candidates could be selected based on their rate of DNA damage accumulation and repair, as measured by comprehensive multi-omic analyses[1], or prioritizing those with lower rate of mutations measured with clonal hematopoiesis (CH).

However, additional clues and protective mechanisms can be gleaned from studies on bacteria and multicellular extremophiles. Studies on various bacteria have shown increases in mutation rates as well as increases in virulence, antibiotic resistance, metabolic activity, shorter lag phase time, and a number of beneficial adaptations in response to short orbital flights[8]. Bacteria such as *Deinococcus radiodurans* have increased radiotolerance via enhanced and efficient DNA repair systems and protection of protiens[10,11]. Many radiotolerant species have the ability to enter anhydrobiotic states for extended periods of time and so there is a selective pressure to withstand endogenous reactive oxygen species generated during times of desiccation[3,5,12,13]. As such, desiccated tardigrades of the species *R. coronifer* and *M. tardigradum* have been shown to survive the combined effects of the vacuum of space, galactic cosmic radiation on the scale of 9.1Gy, and different spectra of UV radiation at a total dose of 7577kJ/m^2 at low earth orbit[3,5,12,13].

Anhydrobiosis in tardigrade species *R. varieornatus* has been shown to provide better aid in the prevention of DNA damage accumulation than in the hydrated stage in response to UV-C radiation as measured by UV-induced thymine dimers[16]. However, hydrated tardigrades in

another study were shown to be more resistant to heavy ion radiation than in their anhydrobiotic state as demonstrated as the LD_{50} for heavy ions being 4.4kGy to 5.2kGy for hydrated and dehydrated animals respectively[1]. As the majority of damage of High-LET is deposited along linear tracks to pass right through cells and induce DSBs as opposed to the indirect ROS effects of Low-LET, there could be separate mechanisms for defending against varying types of radiation. An overlap of functional redundancy between proteins of both systems as adult tardigrades of various species have been shown to be just as tolerant to High-LET as they are to Low-LET radiation[1,3,5,13,16,17]. This includes the recently-discovered protein, Dsup[18].

Dsup was found to co-localize with nuclear DNA through its highly basic c-terminal domain. This region was later discovered to have a very similarly conserved protein sequence with the vertebrate HMGN family of proteins in its RRSARLSA consensus found in the nucleosome binding domain of both proteins[19]. The current proposed mechanism for which Dsup prevents DNA damage is that it suppresses DNA breaks and acts as a physical protectant against damage inducing agents[18,20]. It is also possible that Dsup may act functionally similar to HMGN in terms of enhancing DNA repair mechanisms in addition to its shielding effect[19], but there is no functional genomics data to yet verify this hypothesis. Indeed, the HMGN proteins colocalize with epigenetic marks of active chromatin, but also promote chromatin decompaction via competitively binding with H1, perhaps similar to how Dsup interacts with nucleosomes[19,24,25,26].

Understanding the molecular mechanisms underpinning extremophile tolerance could provide us clues on how human survival in space could be improved through genetic engineering. However, it is essential to understand how introducing a foreign gene from one species to another affects the overall system. Here, we developed a lentiviral-transduced HEK293 cell line containing Dsup (HEK293-Dsup) from which we created a clonal cell line to test functional assays that measure biomarkers indicative of DNA damage. We then performed RNA-seq analysis on these cell lines at various doses of radiation and time points in order to understand the dynamics of how Dsup responds to radiation in the context of human cells. These data show overall high functionality of the radioprotective effects, with some changes in overall gene expression, and also provide a resource of data on human cell regulatory changes when utilizing the foreign Dsup protein.

Results

Confirmation of presence of Dsup in HEK293 cells and integration into chromosome 5

After transduction of pLVX Puro Dsup into HEK293 cells, Dsup protein expression was confirmed via western blot analysis using an HA tag antibody and visualized as a band at 43kDa along with the larger 110kDa vinculin housekeeping gene **(Supplemental Figure S1a)**. Vinculin was present in all cell types but only HA tagged antibodies were present in HEK293-Dsup. Dsup expression was also later confirmed in Fgsea from DESeq2 results **(Supplemental Figure S1b)**. Dsup remains stably expressed in terms of TPM across all time points and doses of radiation but not in control HEK293 cells, further validating the expression of Dsup in our engineered cell line. Next, long read PromethION Nanopore sequencing was done to determine integration site of pLVX-Puro Dsup. The complete pLVX-Puro Dsup vector plasmid was used as a reference for mapping of long reads to the reference HEK293 genome. 1,043,859 reads were obtained with a median of 3,573 reads for HEK293 Dsup with 98% of reads maps and 1.1x genome coverage. According to FindGenomics digital karyotyping service analysis, our cell lines matched to

137 HEK293 reference as outlined in Lin et. al[65]. Accordingly, part of the pLVX Puro Dsup vector
138 mapped to the right arm of chromosome 5 further confirming Dsup lentiviral integration
139 (**Supplemental Figure S2**).
140
141 *Measuring apoptosis*
142 We sought to look at apoptosis by luciferase fusion annexin V binding of phosphatidylserine. We
143 detected early apoptosis in live cells measured over the span of 48hrs as a measure of relative
144 luminescence units for different doses of radiation and 100μM of H_2O_2 (**Figure 1a**). For the 1hr
145 post treatment cells, there were already significant differences (p=0.01) between controls and
146 Dsup cells, with control HEK293 cells displaying significantly more apoptotic signals at 2Gys of
147 radiation and up. About twice as much apoptotic signal was detected up until 6hrs later for
148 control cells as compared to HEK293-Dsup, except the only significant difference between H_2O_2
149 treatment was at 1hr post treatment, indicating perhaps a different mechanism of ROS damage
150 response for Dsup-expressing cells. At 24hrs, this signal began to become saturated and only at
151 higher doses of radiation again were these signals significant. Interestingly, at 48hrs HEK293-
152 Dsup no longer had less apoptotic signal than HEK293 cells at 1Gy, 2Gy, and 4G. Notably, at
153 0Gy, apoptotic signaling continued to rise over time for both control and HEK293-Dsup cells,
154 indicating that perhaps natural baseline apoptotic signaling pathways are still functional in
155 response to a stress free environment[60], but nevertheless diminished in HEK293-Dsup after a
156 certain time post seeding of cells. In conjunction with PS annexin V binding, Dsup expressing
157 cells also showed significantly less (p = 0.009) apoptotic activity as measured by Casapase-3
158 activity over a time frame of 22.5 hours (**Figure 1b & 1c)**.
159
160 *Differential expression profiling*
161 In order to probe how integration of Dsup affects gene expression and regulatory pathways, we
162 subjected HEK293 control cells and HEK293-Dsup cells to varying doses of X-ray radiation and
163 collected cells for RNA-sequencing (RNAseq) library prep across three time points
164 (**Supplemental Figure S3)**, in triplicate. These time points were chosen based off of RNAseq
165 analyses involved in irradiation of human cell lines[66,67] and to observe differences in how these
166 cell lines react initially to radiation stress (0.5, 1, 2, 4 Gy) and overtime through the iterative
167 process of DNA damage repair[49,53]. After differential gene expression analysis was conducted
168 using DESeq2 normalization and GSEA analysis, PCA and t-SNE plots were generated to
169 observe any clustering of genotype, time, and radiation dose. We observed the stronger variance
170 and clustering of time followed by genotype and then radiation dose (**Figure 2**). Accordingly,
171 HEK293 Dsup at 0Gys baseline separated with higher variance from the other groups across the
172 three timepoints, indicating differences in baseline expression between Dsup expressing cells and
173 controls. When comparing genotypes at individual hours, clustering can be seen more clearly
174 between HEK293-Dsup and controls.
175
176 Similarly, differences in gene expression was observed in volcano plots for each timepoint. Here
177 we see that DSUP is the most upregulated gene across all time points in terms of adjusted p-
178 value and $\log_2$ fold change. Overall we observed more upregulation of genes in Dsup-expressing
179 cells (63%) compared to controls when all time points are analyzed at once **Figure 3b.** Across
180 each time point including each dose of radiation however, there appears to be more differential
181 gene expression occurring later at 6hrs and 24hrs as compared to 1hr post irradiation
182 (**Supplemental Figure S5b,d,e**). Heatmaps in **Figure 4a.** reveal a similar pattern of differential
183 expression. Here we see differential signatures at 1hr post irradiation **(Figure 3a &**

Supplemental Figure S4a) at 0Gy, 0.5Gy, and 1Gy for HEK293 cells that remain consistent until higher doses of radiation at 2Gy and 4Gy. The opposite pattern is seen in HEK293 Dsup cells at 1hr, but begin to look more like control cells at higher doses of 2Gy and 4Gy of radiation. At 6hrs (**Supplemental Figure S4c**) and 24hrs (**Supplemental Figure S4d)** differences in expression remain the most consistently changed across all radiation doses but differential expression at 0Gys in HEK293 Dsup displays the most dramatically enriched changes in expression as compared to 0Gy baseline HEK293 cells.

Gene set enrichments related to stress response

To assess what baseline expression looks like in HEK293 Dsup cells in comparison to wild type, enrichment analysis was done on just the intersection of genes shared among all three time points. Enrichr was used to generate gene set libraries using a modification of Fishers exact test to generate a combined z-score a p-value in order to rank genes. The Histone Modification gene-set library from ENCODE was analyzed to obtain a gene set library based on histone modifications (**Figure 4a & 4b)**. We separated Running Enrichment Score plots by time for both upregulated and downregulated gene sets. Gene sets were ranked by adjusted p-value correlated with density of genes in each gene set. Downregulated pathways are shown in **(Supplemental Figure S5a).** At 1hr UV damage responses, CD5 targets, and haptotaxis are downregulated while at 6 and 24hrs, UV damage responses, homologous recombination, rRNA metabolic processes, and inflammation responses are down. (**Supplemental Figure S5b).** At 1hr, Zinc Finger Protein target genes, nucleic acid binding, and metastasis related gene sets were upregulated, while at 6 and 24hrs inflammation, growth regulation, and hypoxia responses were upregulated. The intersection for all time points of the upregulated and downregulated gene sets were also analyzed. **Figure 4c** shows mostly a downregulation of gene sets belonging to ubiquitin protein ligases, nuclear protein import, and whole sets of certain chromosomal regions corresponding to ch13q14 and chr2q33. **Figure 5d** shows a shared upregulation of chromatin modulators involved with histone methylation and zinc finger protein targets.

Enriched KEGG pathways

Next we looked at overall differential expression between HEK293 Dsup cells and WT HEK293 cells. This included gene set enrichment analysis for all time points and doses of radiation combined. Here, we ranked our multivariate DESeq2 results by adjusted p-value multiplied by Log_2FC (<0.05 for p-adjusted and >1.5 for Log_2FC). For biological process we see an upregulation of metabolism, response to stimuli, and growth and cell proliferation (**Figure 5a, 5b, 5c)**. A few of the top cellular component categories included cell membrane, nucleus, and membrane-enclosed lumen. For molecular function, we observed significant enrichment of protein binding, ion binding, and nucleic acid binding gene sets, as well as chromatin binding, antioxidant activity, and oxygen binding. Of note, the top upregulated pathways included many that are common in cancerous phenotypes that are resistant to different types of therapy including radiation therapy. We also see up regulation of lipolysis, a common stress response in exposure to oxidation and ionizing radiation[14,84]. There is also a downregulation of oxidative phosphorylation, indicative of radiation resistant hypoxic cells[69,70].

As Dsup shares amino acid sequence homology with the high mobility group proteins, in particular HMGN1 and 2, we checked to see if expressing Dsup in HEK293 cells would potentially lead to a perturbance of these expression levels, as they are hypothesized to bind to the same nucleosome structures[19]. Using our DESeq2 input and running Fsgea, TPM was

counted for each of the HMGN1 and 2 proteins. While levels of transcripts appear to fluctuate across different doses of radiation and time, both genes were still found to be stably expressed in HEK293 Dsup cells as compared to controls **(Supplemental Figure S6)**.

Discussion

Chromosomal aberrations due to GCR-induced DSBs can be a major detriment to future long-duration space flight missions. In the NASA Twins Study data, a greater rate of chromosomal inversions were found during space flight, and after, indicating genomic instability and rearrangement[8]. Since the tardigrade Dsup protein has been shown to suppress DNA damage we tested if a stably-transfected human cell line could also sustain such protective phenotypes, and if there would be other changes to human gene expression networks. Overall, the results validate the functional radioprotective capacity of Dsup in human cells, to establish the stable line for use by others, and provide new molecular details about the functional genomic impact of Dsup integration into the human genome.

Interestingly, there were significant upregulated enrichments in DSUP expressing cells for pathways associated with histone H3 acetylation and methylation. Specifically, an upregulation of both the gene signatures of the repressive mark H3K27me3 and the active mark H3K4me3 indicative of bivalent gene targets associated with EZH2, the catalytic subunit of PRC2. These findings support the model that Dsup binds to nucleosomes and remodels chromatin as an architectural chromatin protein similar to its homologous counterparts the HMGN proteins[19]. This same expression pattern from our dataset was also observed in a study where HMGN1 was overexpressed in Ts1Rhr mouse models where EZH2 targets and H3K27ME3 pathways were significantly enriched in overexpressing HMGN1 cells as compared to wild type[27]. This could be the result of overexpression of chromatin architectural proteins as TPM normalization of HMGN1 appears stable in DSUP expressing cells.

Of note, as damage from radiation increased, so did many of our top pathways at 1hr post irradiation involving HAT activity. It has been demonstrated in multiple *in vivo* and *in vitro* models that cells lacking high mobility group proteins are far more sensitive to radiation and other damaging agents as these chromatin architectural modifiers are shown to enhance the recognition and processing of DNA damage by making DNA lesions more accessible to repair machinery[36,37,38]. With the decompaction of chromatin, High Mobility Group proteins also induce kinks in exposed DNA in order to make these sites more accessible as well. Given that Dsup is about 4 times as large as HMGN1, it is possible that Dsup could confer human cells with greater chromatin decompaction and accessibility to sites of damage[19,38], or work with other proteins to accomplish such reorganization.

Strikingly, these patterns of chromatin remodeling pathways also move together with an upregulation of DNA damage repair and response pathways within 1hr of radiation and become more pronounced with greater doses. Here we see even at 0.5Gy and 1Gy of radiation an upregulation of characteristic radiation damage response pathways[39]. At higher doses of 2Gy and 4Gy there is a more pronounced upregulation of multiple damage response pathways that include upregulation of members of double strand break and repair pathways[40-46]. In addition, a number of other Zinc Finger protein targets were upregulated, which could be indicative of an enhanced DNA damage repair process[73]. GSEA of KEGG pathways also showed an upregulation of

277 lipolysis, a known protective metabolism stress response of both humans and tardigrades[14,84].
278 Long fatty acid chains can often serve as damage response signaling molecules and can regulate
279 inflammation as well as mediate recovery after injury[84]. Fatty acid metabolism was shown to be
280 affected dynamically by space flight in the NASA Twin study and as such, spikes in midflight
281 expression levels of genes in the lipolysis regulation pathways were upregulated[84].
282
283 Cell cycle checkpoint pathways, such as those belonging to the DNA damage response CHEK2
284 network, also became upregulated in response to higher doses at 1hr as well as the ANP32B
285 pathway necessary for cell cycle progression from G1 to S phase[47,48]. Dsup-expressing cells
286 could move through cell cycle progression phases faster than wild type cells because of an
287 increased rate of damage clearance that's necessary to enter the next cell cycle phase. DNA
288 damage repair is an iterative process and cells enter a state of senescence until the damage is
289 repaired sufficiently or if the accumulation of damage is beyond repair then apoptotic pathways
290 are triggered[49].
291
292 Given these broad results, one can imagine Dsup and related genes helping in the creation of a
293 temporal, radiation, or molecule controlled, inducible Dsup system that is activated in response
294 to intense periods of galactic cosmic radiation. Indeed, such work has already begun for atomic
295 energy workers and in other trials of engineered cancer therapies that leverage CRISPR[85]. Even if
296 not directly used as a therapeutic, the gene expression perturbation data here, as well as the
297 stably-expressing cell line, can serve as resources to guide future research on radioresistance and
298 baseline levels of transcriptional disruption after the stable integration of a radioresistance gene.
299 Together, such tools and data sets will help keep astronauts safer as missions move farther from
300 Earth, become riskier, and are laden with ever-increasing levels of GCR and irradiation.
301
302 **Methods**
303 *Plasmid Design and Extraction*
304 The complete coding sequence for DSUP from *Ramazzottius varieornatus* as described in
305 Hashimoto et. Al was obtained from The Kumashi Genome Project database. This sequence was
306 cloned into a custom pLVX Puro plasmid lentiviral vector with a constitutive CMV promoter.
307 Dsup was ligated into the 5' EcoR1 and 3' XbaI in the multiple cloning site of pLVX Puro.
308 GeneWiz® Gene synthesis services was used to codon optimize DSUP for expression in
309 mammalian systems. An influenza Hemagglutinin tag was synthesized on the N-terminal region
310 of DSUP to minimize interference of c-terminal binding of DSUP to nucleosomes and for
311 downstream antibody detection.
312
313 The plasmid was then transformed into DH5α Competent Cells. 10ng of DSUP pLVX Puro
314 plasmid was added to 100µl of competent cells and incubated on ice for 30mins followed by heat
315 shock for 45 seconds in a 42°C water bath and then incubated on ice for 2mins. 900µl of S.O.C.
316 medium was added to cells and shook at 225rpm at 37°C for 1hr before 100ul were spread using
317 glass beads on LB 100µg/ml ampicillin plates. Plates were incubated overnight at 37°C and
318 colonies were picked the following day for miniprep. Multiple colonies were picked and grown
319 in 4mls of LB broth containing 100µg/ml of ampicillin shaking overnight at 250rpm and 37°C.
320 DNA from cultures were extracted the following day using Promega™ Wizard® Plus SV
321 Miniprep kit. Plasmid DNA was eluted from spin columns in 30µl of nuclease free water.
322

323 500ng of plasmid DNA sample was restriction enzyme digested in NEB 10X CutSmart® Buffer
324 with 1μl of EcoRI and XbaI at 37°C for 3hrs before run on a gel using NEB 6X loading dye and
325 Invitrogen™ 1KB plus DNA ladder for 45mins at 130V. Samples cut at 1377 Bps corresponding
326 to DSUP and 8069 base pairs corresponding to pLVX Puro vector backbone were chosen for
327 maxiprep using Invitrogen™ PureLink™ HiPure Plasmid Filter Maxiprep Kit. The correctly
328 digested sample was grown in 500mls of LB with 100μg/ml ampicillin overnight shaking at
329 250rpm at 37°C. In parallel pLVX Puro empty vector, pMD2.G VSV-G envelope plasmid, and
330 psPAX2 lentiviral packaging plasmid transformed and extracted using the above protocols were
331 also grown overnight up for maxiprep. 300μl of nuclease free water was passed through the
332 precipitator to elute the plasmid DNA into 1.5ml Eppendorf microcentrifuge tubes. Plasmid
333 DNA was then quantified using Qubit™ 1X dsDNA HS assay. 1μg and above was quantified for
334 each plasmid DNA sample.
335
336 *Generation of lentiviral transduced stable HEK293 DSUP Cell line*
337 HEK293 cells and HEK293T cells at passage 13 and 17 respectively were donated by Dr. Levitz
338 at Weill Cornell were grown and incubated at standard incubation conditions at 37°C with 5%
339 CO_2 in complete DMEM media supplemented with 10% FBS, 1% Pen/Strep, and 1X Glutamax
340 on T-75 Nunc™ EasYFlasks™. HEK293T cells were split at 1:10 and $2.2x10^6$ cells were seeded
341 on two PLL coated 100mm plates for transfection of pLVX Puro DSUP and empty vector pLVX
342 Puro as an empty vector control for downstream experiments.
343
344 Mirus TransIt® Lentivirus System was used to transfect 80-95% confluent HEK293T cells
345 grown the previous day in Opti-MEM reduced serum media. TransIT® Lenti Reagent was
346 warmed to room temperature and vortexed gently before using. 200μl of Opti-Mem™ media was
347 added to sterile 1.5ml Eppendorf microcentrifuge tubes while 1.65 pmol of either pLVX Puro
348 DSUP or empty vector pLVX Puro was combined with 1.3pmol of psPAX2 plasmid and
349 0.72pmol of pMD2.G plasmid. 2μg of plasmid mixture was then transferred to the tube
350 containing Opti-MEM. 6μl of TransIT®-Lenti Reagent was added to the diluted plasmid DNA
351 mixture and incubated for 10mins at room temperature. The mixture was then added dropwise to
352 different areas of the plate and gently rocked back and forth to ensure even distribution. Plates
353 were stored at 37°C with 5% CO_2 for 48hrs before packaged lentivirus particles were harvested.
354 Viral particles were filtered through a 10ml syringe with a 0.45μm PVDF filter and separated
355 into 1ml aliquots to be flash frozen and stored in -80°C.
356
357 Mirus TransduceIT™ Reagent was used to efficiently transduce HEK293 cells plated on 100mm
358 plates at a density of $2.2x10^6$ cells seeded the previous day. TransduceIT™ Reagent was added to
359 the HEK293 cells along with 1ml of virus particles distributed evenly over the plate dropwise.
360 Cells were incubated for 48hrs before being selected with 2μg/ml of puromycin as determined by
361 puromycin kill curve analysis on WT HEK293 cells. After 1 week of selection HEK293 DSUP
362 and HEK293 empty vector cells were obtained and expanded on T-75 flasks.
363
364 Serial dilution cloning was performed on HEK293 Dsup cells in order to obtain clonal cell lines.
365 200μl of cell suspension at $2x10^4$ was added to the first well A1 of a 96 well plate. 100μl of
366 complete DMEM media was added to each well except A1 using a multichannel pipette. Using a
367 single channel pipette 100μl of cell suspension was added below to well B1 and mixed before

368 100µl of that cell suspension was added to the next well below it until dilutions were made to
369 well H1. Then using a multichannel pipette 100µl of those cell suspensions were added to the
370 next columns further creating serial dilutions that would span across the plate. Cells were
371 incubated at standard conditions and after 5 days individual clones were isolated in some wells
372 as detected by microscopy. Once these wells were confluent, they were treated with trypsin and
373 resuspended in complete DMEM media to be expanded on 24 well plates followed by 6 well
374 plates, T-25 flasks, and finally T-75 flasks.
375
376 *Western Blot*
377 Confirmation of Dsup was assessed by western blot. HEK293 Dsup, HEK293 empty vector, and
378 HEK293 cells were plated in triplicates on 100mm dishes at a seeding density of $2.2x10^6$ cells
379 per dish. The following day after incubation the dishes were placed in ice and washed with ice
380 cold Tris-buffered saline. The TBS was aspirated and 1ml of ice-cold RIPA buffer was added to
381 dissolve cell membranes. Cell lysates were collected in 2ml pre-cooled Eppendorf tubes.
382 Constant agitation was maintained at 1400rpm for 30mins and 4°C before being spun down at
383 16,000xg for 20mins at 4°C. The supernatant was transferred to a new pre-cooled
384 microcentrifuge tube and 10µl of lysate was used to determine protein concentration using
385 Qubit™ Protein Assay kit. 20ug of each sample was then added to an equal volume of 2x
386 Laemmli sample buffer before being boiled at 95°C for 5mins. Equal amounts of protein along
387 with a PageRuler™ Plus Pre-stained protein ladder were loaded into a Bio-Rad 10 well 4-20%
388 Mini-PROTEAN® TGX™ Precast Protein Gel. Protein separation by electrophoresis was then
389 performed in a Mini PROTEAN Tetra cell with 1liter of Tris/Glycine/SDS running buffer. The
390 gel was run a 50V for 5mins and then 100V for 1hr.
391
392 The gel was then placed in 1X transfer buffer for 15mins and the transfer sandwich was
393 assembled using a 0.20µm Nitrocellulose membrane and sponges. The assembled transfer
394 sandwich was placed in the transfer cassette and proteins were transferred for 1hr at 100Volts
395 and 350mA current in the Mini PROTEAN Tetra cell with 1L of transfer buffer. The blot was
396 briefly rinsed with Millipore water and stained with Ponceau S solution to confirm transfer of
397 proteins. The blot was then rinsed three times with 1X TBST and blocked in 5% milk in 1X
398 TBST at room temperature for 1hr. R&D Systems recombinant mouse HA Tag antibody
399 (MAB0601) and control Bio-Rad Mouse anti Human Vinculin antibody (V284) was diluted to a
400 working concentration of 0.1µg/ml and a 1:500 dilution in 1% milk in 1X TBST respectively and
401 the primary antibodies were incubated on the membrane overnight at 4°C. The following day the
402 blot was rinsed 5 times for 5mins each with 1X TBST before adding the Invitrogen Goat anti-
403 Rabbit IgG (H+L) Cross-Absorbed Secondary Antibody DyLight 800 (SAS-10036) and Rabbit
404 anti-Mouse IgG (H+L) Cross-adsorbed Secondary Antibody Alexa Fluor Plus 680 (A32729)
405 diluted to working concentrations of 1:5000 dilution and 0.1µg/ml respectively in 1% milk in 1X
406 TBST. The blot was incubated at room temperature for 1hr, rinsed 5 times for 5 mins in 1X
407 TBST and then imaged on a Li-Cor Odyssey® CLx imagine system using both 700nm and
408 800nm channels.
409
410 *Confirmation of lentiviral insertion site using Oxford Nanopore long read sequencing*
411 DNA from HEK293 Dsup cell line at passage 20 and 22 and the parental HEK293 cell line at
412 passage 18 were extracted using Trizol as mentioned above. Briefly, at phase separation ethanol
413 was added to the lower phenol-chloroform phase and interphase, centrifuged and pelleted, and

414 resuspended in sodium citrate. After 2 wash steps with 75% ethanol, the DNA pellet was allowed
415 to air dry and then resuspended in 8mM NaOH. DNA concentration was assessed via QuBit 1X
416 dsDNA assay and prepared for long read sequencing using the Ligation Sequencing Kit (LSK-
417 109) for Oxford Nanopore. The adapter ligated gDNA was sequenced using a PromethION flow
418 cell and base called in real time using Guppy 3.4. The data was analyzed using FindGenomics
419 digital karyotyping service.
420
421 *Cell Irradiation*
422 Cells were incubated overnight post seeding at 37°C with 5% CO_2 before irradiation. The
423 following day cells were taken out of the incubator and subjected to X-rays in a Rad Source
424 Technologies RS 2000 Biological research irradiator and irradiated at 1Gy, 2Gy, 4Gy, and 16Gy
425 while the corresponding 0Gy plate was kept outside the incubator as a no treatment control. For
426 the RNAseq experiment, cells were irradiated at 0.5Gy, 1Gy, 2Gy, and 4Gy. Dose time was
427 determined divided by the dose rate of 2Gy/min.
428
429 *Annexin V Apoptosis Assay*
430 Live cell real time monitoring of apoptosis was conducted using Promega RealTime-Glo™
431 Annexin V Apoptosis Assay. HEK293, HEK293 Dsup, and HEK293 empty vector cells were
432 seeded on 6 separate 96 Well White Polystyrene microplates at a density of 1,000 cells/well at a
433 volume of 100µl in triplicates and incubated at 37°C with 5% CO_2 overnight. 100µl of complete
434 medium were added to wells not containing cells as no cell and no compound controls. Each
435 plate was a separate treatment condition and each row contained all cell types in triplicates and
436 corresponded to a different time point from which apoptosis would be assayed.
437
438 The following day cells were taken out of the incubator and subjected to X-ray irradiation and
439 hydrogen peroxide treatment as indicated above. Apoptosis was assessed at 1hr, 6hrs, and 24hrs
440 post irradiation. To prepare the 2X detection reagent, 1000X Annexin NanoBiT® substrate was
441 added to prewarmed DMEM complete medium at a 500-fold dilution. 1000X $CaCl_2$ was then
442 added to combined DMEM complete medium with diluted NanoBiT® substrate at a 500-fold
443 dilution. 1000X Annexin V-SmBiT and 1,000X Annexin V-LgBiT was added at a 500-fold
444 dilution to the combined substrate, $CaCl_2$, complete medium and was inverted gently a few times
445 to mix. 100µl of the 2X detection reagent was then added to each 96 well plate using a
446 multichannel pipette and mixed at 700rpm for 30 seconds on a plate shaker. Luminescence and
447 fluorescence at $485nm_{Ex}/525\text{-}530nm_{Em}$ data were measured on a Promega™ Glowmax® Plate
448 Reader.
449
450 *Microscopy for Caspase-3 assay:*
451 HEK293 cells containing the Empty Vector, DSUP, or no construct were cultured in DMEM
452 supplemented with 10% FBS. Cells were washed once with PBS before trypsinization. 5 mL of
453 Trypsinized cells were transferred to 10 mL of FluoroBrite DMEM supplemented with 10% FBS
454 and 1% 100x glutamax in a 15 mL conical tube. Cells were pelleted at 330 xg for 3 min. Media
455 trypsin mix was removed before resuspending the cell pellet in 5 mL of the FluoroBrite DMEM
456 described above. 10 µL of resuspended cells were added to 10 µL of trypan blue from the BioRad
457 Cell counting kit. 10 µL of this cell trypan mix was added to a cell counting slide from the same
458 kit. The slide was placed in a TC20™ Automated Cell Counter for cell counting. Based on the
459 count of live cells, each cell line was diluted to 75 cells/µL in the FluoroBrite DMEM described

460 above. 200 µL of this mix was added to each well of a Corning 3603 96 well microscopy grade
461 plate for a total of 15,000 cells per well. The Plate was spun at 330 xg for 3 min. The plate was put
462 in a humidified 37°C incubator with 5% CO_2 for 4 hours to allow cell adherence to the bottom of
463 the well.
464
465 After cell adherence, plates were removed from the incubator and inoculated with 10 µL of a mix
466 containing 105 µM Hoechst 33342 (diluted from Thermo H3570), 26.25 µM Caspase dye (Diluted
467 from Sartorius 4440), and 277.2 µM Camptothecin (diluted from Millipore Sigma C9911) in water.
468 This inoculation amounts to 5 µM Hoechst 33342, 1.25 µM Caspase dye, 13.2 µM Camptothecin
469 in the well. The plate was sealed with a Breathe-Easy® sealing membrane before incubating for
470 30 min in the same incubator described above.
471 After incubation, cells were placed in a humidified 37°C ImageXpress Micro Confocal High-
472 Content Imaging System with 5% CO_2. All wells of the plate were imaged with a 10x Plan Apo
473 Lambda lenses in wide field mode. 9 fields from each well were collected with a 4 ms DAPI
474 exposure and a 93 ms FITC exposure. This process was repeated every 45 min for 22.5 hours (30
475 time points).
476
477 Images were analyzed using MetaXpress. Briefly nuclei were segmented using the built-in find
478 round objects function applied to the DAPI channel. The local background of these objects was
479 defined by using the expand objects without touching function (with the ultimate option
480 checked). The difference between the expanded objects and the nuclei was used to define the
481 background area. The average FITC intensity was calculated for the background and for the
482 nuclear regions. The difference between the nuclear and background FITC intensity was
483 calculated and used as the Caspase signal for each cell at each time point. Upon inspection of the
484 distribution, a cutoff value of 650 caspase signal units was determined to be an appropriate cutoff
485 for cell death as there was a bimodal break around that signal intensity. Cells with lower than
486 650 units of caspase signal were called non-apoptotic, cells with greater than 650 units of
487 caspase signal were considered apoptotic. The percentage of apoptotic cells was calculated for
488 every well at every time point. These points were plotted for all wells tested for each cell line. A
489 bar graph was made with error bars at 1 standard deviation of the apoptotic rate of the cells at the
490 final time point (22.5 h post inoculation). A heterostatic two tailed student t-test was performed
491 to test the null hypothesis that the Empty Vector and DSUP containing cell lines have equal
492 apoptotic rates.
493
494 *RNA sequencing and Differential Gene Expression Analysis*
495 Each cell type was harvested from T-175 at around 75% confluency. Viability and cell count
496 were assessed using TrypanBlue stain on a Countess™ Automated Cell Counter. Each cell type
497 had over 90% viable cells and were then seeded onto 6 well round bottom plates in triplicates for
498 each cell type, treatment, and time point at a density of 30,000 cells/well. Cells were irradiated
499 the following day post seeding at 0.5Gy, 1Gy, 2Gy, and 4Gy of X-rays while 0gy of no treatment
500 controls were kept outside the incubator for the duration of radiation treatment. Cells were
501 incubated at standard cell culture conditions and harvested at 1hr, 6hrs, and 24hrs post treatment.
502
503 A total of 93 samples were selected for NEBNext® Ultra™ II RNA library prep. These include 3
504 HEK293 DSUP replicates x 3 time points x 4 radiation doses + 3 0gy Controls. The same was
505 done for HEK293 cells and 3 HEK293 empty vectors at 2Gy and 6hrs were included. Media was

aspirated, washed once with 1xPBS, and cells were detatched with trypsin before being resuspended and collected into 2ml Eppendorf tubes to be spun down at 6,000xg and pelleted. Media was aspirated and then the cell pellet was resuspended and dissolved in Trizol. Trizol extractions were performed as mentioned above but this time RNA was isolated carefully from the upper aqueous layer and pelleted before being eluted in 30µl of RNAse free water. RNA concentration was measured using Qubit™ HS RNA assay and RIN and fragment distribution was obtained using Agilent High Sensitivity RNA ScreenTape System for TapeStation 2200. RIN was above 9 for all samples and 250ng of RNA sample was brought forward for rRNA ribosomal depletion using NEBNext® rRNA Depletion Kit for human/mouse/rat samples. Following depletion, RNA samples were library prepped and adapter ligated with single Index Primer set 1 NEBNext® Multiplex Oligos for Illumina®. Libraries were then sequenced at 40 million single end 100bp reads on Novaseq 6000.

Read alignment

Libraries were single end 100bp sequenced on NovaSeq6000, targeting 40 million reads. Raw data was base called using Illumina Basespace. GTF and FASTA files for the human reference genome (GRCh38) were downloaded from ENSEMBL. Both GTF and FASTA files were edited to contain the sequence for the protein coding tardigrade gene DSUP. After a reference index was created using STAR (ver 2.7), the reads were then mapped to the human genome[76]. The output BAM files were then sorted using Samtools[78]. Read counts were obtained using Feature Counts in which multi-mapped reads were removed [77].

Normalization using DESeq2

The variance mean was estimated and differential expression was computed using a negative binomial distribution using DESeq2 from raw read count data. First a count matrix was generated and for each gene a general linearized model is fitted. Read counts are then modeled as a negative binomial distribution and the mean is taken as a quantity that is proportional to the concentration of DNA fragments from the gene in the sample and scaled by a normalization factor. The corresponding size factors are then computed using a median on ratios method. When comparing two groups the GLM fit returns coefficients that's indicates the expression strength of a gene and its corresponding Log_2FC. Empirical Bayes shrinkage was used to estimate dispersion parameters within groups to assess for variability between replicates and for shrinkage of fold change estimation to then rank genes. To test for differential expression, DESeq2 uses a Wald test which returns a z-statistic and p-values from a subset of genes that are adjusted using multiple testing via Benjamini and Hochberg correction[79].

Fgsea analysis

Fgsea, a Bioconductor R-package, was used to obtain pre-ranked expression to identify classes of overrepresented genes[64]. Predefined gene sets from MsigDB were grouped together by their involvement in the same biological pathway or by location on chromosome[80]. Features were ranked by differential expression analysis adjusted p-value with corresponding Log_2FC to get normalized enrichment scores. First an enrichment score was calculated by running a sum statistic on each gene in the set to assess the degree to which overrepresented gene sets at the top and bottom of the ranked list deviates from zero using a weighted Kolmogorov-Smirnov like statistic. Then the significance levels of the enrichment scores were calculated to get nominal p-values by calculation of cumulative gene set enrichment values. Last normalized enrichment

scores (NES) are returned by normalizing each enrichment score by the size of the gene set and then the proportion of false positives are controlled by calculating the FDR[81].

Enrichr analysis

Common genes among different time points for 0Gys of radiation were obtained as the intersection of all genes across the three timepoints. Erichr was used to identify enriched gene sets using a hypergeometric model. To compute enrichment, Enrichr uses the Fisher exact test and then computes a mean rank and standard deviation from the expected rank for the terms in the gene set library. A z-score for deviation can also then be computed using a lookup table for expected ranks with associated variances, the output of which is then used as corrected score for ranking terms. In addition, Enrichr also can combine the computed p-value from the Fisher exact test with the z-score of the deviation from the expected rank by multiplying log(p) by z to get c the combined score[74,75].

WebGestalt analysis

To observe overall effect of Dsup in human cells, KEGG pathways were visualized with the web based integrative data mining system WebGestalt[83]. Input data set from DESeq2 was ranked by adjusted p-value multiplied by Log_2FC with a p-value cutoff of 0.05 and Log_2FC cutoff of 1.5 and used for pathway enrichment analysis. This list of genes of interest was then compared to a reference gene set in KEGG using a hypergeometric test to assess the significance of enrichment for a category in the input gene set. The hypergeometric test then provides for an over and underrepresentation of individual genes. Gene sets can then be explored and organized using visualization interfaces through KEGG tables[82,83].

References

1. Cortese, F., Klokov, D., Osipov, A., Stefaniak, J., Moskalev, A., Schastnaya, J., Cantor, C., Aliper, A., Mamoshina, P., Ushakov, I., Sapetsky, A., Vanhaelen, Q., Alchinova, I., Karganov, M., Kovalchuk, O., Wilkins, R., Shtemberg, A., Moreels, M., Baatout, S., Izumchenko, E., … Zhavoronkov, A. (2018). Vive la radiorésistance!: converging research in radiobiology and biogerontology to enhance human radioresistance for deep space exploration and colonization. *Oncotarget*, *9*(18), 14692–14722. https://doi.org/10.18632/oncotarget.24461
2. Cucinotta, F. A., Kim, M. H., Chappell, L. J., & Huff, J. L. (2013). How safe is safe enough? Radiation risk for a human mission to Mars. *PloS one*, *8*(10), e74988. https://doi.org/10.1371/journal.pone.0074988
3. Jönsson K. I. (2019). Radiation Tolerance in Tardigrades: Current Knowledge and Potential Applications in Medicine. *Cancers*, *11*(9), 1333. https://doi.org/10.3390/cancers11091333
4. Gusev, O., Nakahara, Y., Vanyagina, V., Malutina, L., Cornette, R., Sakashita, T., Hamada, N., Kikawada, T., Kobayashi, Y., & Okuda, T. (2010). Anhydrobiosis-associated nuclear DNA damage and repair in the sleeping chironomid: linkage with radioresistance. *PloS one*, *5*(11), e14008. https://doi.org/10.1371/journal.pone.0014008
5. Rizzo, A. M., Altiero, T., Corsetto, P. A., Montorfano, G., Guidetti, R., & Rebecchi, L. (2015). Space flight effects on antioxidant molecules in dry tardigrades: the TARDIKISS

experiment. *BioMed research international*, *2015*, 167642. https://doi.org/10.1155/2015/167642

6. Daly, M. J., Gaidamakova, E. K., Matrosova, V. Y., Vasilenko, A., Zhai, M., Leapman, R. D., Lai, B., Ravel, B., Li, S. M., Kemner, K. M., & Fredrickson, J. K. (2007). Protein oxidation implicated as the primary determinant of bacterial radioresistance. *PLoS biology*, *5*(4), e92. https://doi.org/10.1371/journal.pbio.0050092
7. Wang, L., He, L., Bao, G., He, X., Fan, S., & Wang, H. (2016). Ionizing Radiation Induces HMGB1 Cytoplasmic Translocation and Extracellular Release. *Guo ji fang she yi xue he yi xue za zhi = International journal of radiation medicine and nuclear medicine*, *40*(2), 91–99.
8. Taylor, L., Vitaterna, M. H., Afkarian, M., Afshinnekoo, E., Ahadi, S., Ambati, A., … Turek, F. W. (2019). The NASA Twins Study: A multidimensional analysis of a year-long human spaceflight. *Science (New York, N.Y.)*, *364*(6436), eaau8650. https://doi.org/10.1126/science.aau8650
9. Taylor P. W. (2015). Impact of space flight on bacterial virulence and antibiotic susceptibility. *Infection and drug resistance*, *8*, 249–262. https://doi.org/10.2147/IDR.S67275
10. Hashimoto, T., & Kunieda, T. (2017). DNA Protection Protein, a Novel Mechanism of Radiation Tolerance: Lessons from Tardigrades. *Life (Basel, Switzerland)*, *7*(2), 26. https://doi.org/10.3390/life7020026
11. Daly, M. J., Gaidamakova, E. K., Matrosova, V. Y., Vasilenko, A., Zhai, M., Leapman, R. D., Lai, B., Ravel, B., Li, S. M., Kemner, K. M., & Fredrickson, J. K. (2007). Protein oxidation implicated as the primary determinant of bacterial radioresistance. *PLoS biology*, *5*(4), e92. https://doi.org/10.1371/journal.pbio.0050092
12. Gusev, O., Nakahara, Y., Vanyagina, V., Malutina, L., Cornette, R., Sakashita, T., Hamada, N., Kikawada, T., Kobayashi, Y., & Okuda, T. (2010). Anhydrobiosis-associated nuclear DNA damage and repair in the sleeping chironomid: linkage with radioresistance. *PloS one*, *5*(11), e14008. https://doi.org/10.1371/journal.pone.0014008
13. Weronika, E., & Łukasz, K. (2017). Tardigrades in Space Research - Past and Future. *Origins of life and evolution of the biosphere : the journal of the International Society for the Study of the Origin of Life*, *47*(4), 545–553. https://doi.org/10.1007/s11084-016-9522-1
14. Förster, F., Beisser, D., Grohme, M. A., Liang, C., Mali, B., Siegl, A. M., Engelmann, J. C., Shkumatov, A. V., Schokraie, E., Müller, T., Schnölzer, M., Schill, R. O., Frohme, M., & Dandekar, T. (2012). Transcriptome analysis in tardigrade species reveals specific molecular pathways for stress adaptations. *Bioinformatics and biology insights*, *6*, 69–96. https://doi.org/10.4137/BBI.S9150
15. Neumann, S., Reuner, A., Brümmer, F., & Schill, R. O. (2009). DNA damage in storage cells of anhydrobiotic tardigrades. *Comparative biochemistry and physiology. Part A, Molecular & integrative physiology*, *153*(4), 425–429. https://doi.org/10.1016/j.cbpa.2009.04.611
16. Horikawa, D. D., Cumbers, J., Sakakibara, I., Rogoff, D., Leuko, S., Harnoto, R., Arakawa, K., Katayama, T., Kunieda, T., Toyoda, A., Fujiyama, A., & Rothschild, L. J. (2013). Analysis of DNA repair and protection in the Tardigrade Ramazzottius varieornatus and Hypsibius dujardini after exposure to UVC radiation. *PloS one*, *8*(6), e64793. https://doi.org/10.1371/journal.pone.0064793

17. Nilsson, E. J., Jönsson, K. I., & Pallon, J. (2010). Tolerance to proton irradiation in the eutardigrade Richtersius coronifer--a nuclear microprobe study. *International journal of radiation biology*, *86*(5), 420–427. https://doi.org/10.3109/09553000903568001
18. Hashimoto, T., Horikawa, D. D., Saito, Y., Kuwahara, H., Kozuka-Hata, H., Shin-I, T., Minakuchi, Y., Ohishi, K., Motoyama, A., Aizu, T., Enomoto, A., Kondo, K., Tanaka, S., Hara, Y., Koshikawa, S., Sagara, H., Miura, T., Yokobori, S. I., Miyagawa, K., Suzuki, Y., … Kunieda, T. (2016). Extremotolerant tardigrade genome and improved radiotolerance of human cultured cells by tardigrade-unique protein. *Nature communications*, *7*, 12808. https://doi.org/10.1038/ncomms12808
19. Chavez, C., Cruz-Becerra, G., Fei, J., Kassavetis, G. A., & Kadonaga, J. T. (2019). The tardigrade damage suppressor protein binds to nucleosomes and protects DNA from hydroxyl radicals. *eLife*, *8*, e47682. https://doi.org/10.7554/eLife.47682
20. Mah, L., El-Osta, A. & Karagiannis, T. γH2AX: a sensitive molecular marker of DNA damage and repair. *Leukemia* **24,** 679–686 (2010). https://doi.org/10.1038/leu.2010.6
21. Subramanian, M., Gonzalez, R. W., Patil, H., Ueda, T., Lim, J. H., Kraemer, K. H., Bustin, M., & Bergel, M. (2009). The nucleosome-binding protein HMGN2 modulates global genome repair. *The FEBS journal*, *276*(22), 6646–6657. https://doi.org/10.1111/j.1742-4658.2009.07375.x
22. Birger, Y., West, K. L., Postnikov, Y. V., Lim, J. H., Furusawa, T., Wagner, J. P., Laufer, C. S., Kraemer, K. H., & Bustin, M. (2003). Chromosomal protein HMGN1 enhances the rate of DNA repair in chromatin. *The EMBO journal*, *22*(7), 1665–1675. https://doi.org/10.1093/emboj/cdg142
23. He, B., Deng, T., Zhu, I., Furusawa, T., Zhang, S., Tang, W., Postnikov, Y., Ambs, S., Li, C. C., Livak, F., Landsman, D., & Bustin, M. (2018). Binding of HMGN proteins to cell specific enhancers stabilizes cell identity. *Nature communications*, *9*(1), 5240. https://doi.org/10.1038/s41467-018-07687-9
24. Apelt, K., Zoutendijk, I., Gout, D. Y., Wondergem, A. P., van den Heuvel, D., & Luijsterburg, M. S. (2020). Human HMGN1 and HMGN2 are not required for transcription-coupled DNA repair. *Scientific reports*, *10*(1), 4332. https://doi.org/10.1038/s41598-020-61243-4
25. Ding, H. F., Bustin, M., & Hansen, U. (1997). Alleviation of histone H1-mediated transcriptional repression and chromatin compaction by the acidic activation region in chromosomal protein HMG-14. *Molecular and cellular biology*, *17*(10), 5843–5855. https://doi.org/10.1128/mcb.17.10.5843
26. Catez, F., Yang, H., Tracey, K. J., Reeves, R., Misteli, T., & Bustin, M. (2004). Network of dynamic interactions between histone H1 and high-mobility-group proteins in chromatin. *Molecular and cellular biology*, *24*(10), 4321–4328. https://doi.org/10.1128/mcb.24.10.4321-4328.2004
27. Mowery, C. T., Reyes, J. M., Cabal-Hierro, L., Higby, K. J., Karlin, K. L., Wang, J. H., Kimmerling, R. J., Cejas, P., Lim, K., Li, H., Furusawa, T., Long, H. W., Pellman, D., Chapuy, B., Bustin, M., Manalis, S. R., Westbrook, T. F., Lin, C. Y., & Lane, A. A. (2018). Trisomy of a Down Syndrome Critical Region Globally Amplifies Transcription via HMGN1 Overexpression. *Cell reports*, *25*(7), 1898–1911.e5. https://doi.org/10.1016/j.celrep.2018.10.061
28. He, J., Liu, C., Wang, B., Li, N., Zuo, G., & Gao, D. (2015). HMGN5 blockade by siRNA enhances apoptosis, suppresses invasion and increases chemosensitivity to

689 temozolomide in meningiomas. *International journal of oncology*, *47*(4), 1503–1511.
690 https://doi.org/10.3892/ijo.2015.3131
691 29. Subramanian, M., Gonzalez, R. W., Patil, H., Ueda, T., Lim, J. H., Kraemer, K. H.,
692 Bustin, M., & Bergel, M. (2009). The nucleosome-binding protein HMGN2 modulates
693 global genome repair. *The FEBS journal*, *276*(22), 6646–6657.
694 https://doi.org/10.1111/j.1742-4658.2009.07375.x
695 30. Martens, J. H., Brinkman, A. B., Simmer, F., Francoijs, K. J., Nebbioso, A., Ferrara, F.,
696 Altucci, L., & Stunnenberg, H. G. (2010). PML-RARalpha/RXR Alters the Epigenetic
697 Landscape in Acute Promyelocytic Leukemia. *Cancer cell*, *17*(2), 173–185.
698 https://doi.org/10.1016/j.ccr.2009.12.042
699 31. Lu, C., Han, H. D., Mangala, L. S., Ali-Fehmi, R., Newton, C. S., Ozbun, L., Armaiz-
700 Pena, G. N., Hu, W., Stone, R. L., Munkarah, A., Ravoori, M. K., Shahzad, M. M., Lee,
701 J. W., Mora, E., Langley, R. R., Carroll, A. R., Matsuo, K., Spannuth, W. A., Schmandt,
702 R., Jennings, N. B., … Sood, A. K. (2010). Regulation of tumor angiogenesis by EZH2.
703 *Cancer cell*, *18*(2), 185–197. https://doi.org/10.1016/j.ccr.2010.06.016
704 32. McCabe, M. T., Graves, A. P., Ganji, G., Diaz, E., Halsey, W. S., Jiang, Y., Smitheman,
705 K. N., Ott, H. M., Pappalardi, M. B., Allen, K. E., Chen, S. B., Della Pietra, A., 3rd, Dul,
706 E., Hughes, A. M., Gilbert, S. A., Thrall, S. H., Tummino, P. J., Kruger, R. G., Brandt,
707 M., Schwartz, B., … Creasy, C. L. (2012). Mutation of A677 in histone methyltransferase
708 EZH2 in human B-cell lymphoma promotes hypertrimethylation of histone H3 on lysine
709 27 (H3K27). *Proceedings of the National Academy of Sciences of the United States of*
710 *America*, *109*(8), 2989–2994. https://doi.org/10.1073/pnas.1116418109
711 33. Hübner, J. M., Müller, T., Papageorgiou, D. N., Mauermann, M., Krijgsveld, J., Russell,
712 R. B., Ellison, D. W., Pfister, S. M., Pajtler, K. W., & Kool, M. (2019). EZHIP/CXorf67
713 mimics K27M mutated oncohistones and functions as an intrinsic inhibitor of PRC2
714 function in aggressive posterior fossa ependymoma. *Neuro-oncology*, *21*(7), 878–889.
715 https://doi.org/10.1093/neuonc/noz058
716 34. Pasini, D., Bracken, A. P., Jensen, M. R., Lazzerini Denchi, E., & Helin, K. (2004).
717 Suz12 is essential for mouse development and for EZH2 histone methyltransferase
718 activity. *The EMBO journal*, *23*(20), 4061–4071.
719 https://doi.org/10.1038/sj.emboj.7600402
720 35. Gerlitz G. (2010). HMGNs, DNA repair and cancer. *Biochimica et biophysica acta*,
721 *1799*(1-2), 80–85. https://doi.org/10.1016/j.bbagrm.2009.10.007
722 36. Lange, S. S., Mitchell, D. L., & Vasquez, K. M. (2008). High mobility group protein B1
723 enhances DNA repair and chromatin modification after DNA damage. *Proceedings of the*
724 *National Academy of Sciences of the United States of America*, *105*(30), 10320–10325.
725 https://doi.org/10.1073/pnas.0803181105
726 37. Lange, S. S., & Vasquez, K. M. (2009). HMGB1: the jack-of-all-trades protein is a
727 master DNA repair mechanic. *Molecular carcinogenesis*, *48*(7), 571–580.
728 https://doi.org/10.1002/mc.20544
729 38. Birger, Y., West, K. L., Postnikov, Y. V., Lim, J. H., Furusawa, T., Wagner, J. P., Laufer,
730 C. S., Kraemer, K. H., & Bustin, M. (2003). Chromosomal protein HMGN1 enhances the
731 rate of DNA repair in chromatin. *The EMBO journal*, *22*(7), 1665–1675.
732 https://doi.org/10.1093/emboj/cdg142
733 39. da Costa, R. M., Riou, L., Paquola, A., Menck, C. F., & Sarasin, A. (2005).
734 Transcriptional profiles of unirradiated or UV-irradiated human cells expressing either

735 the cancer-prone XPB/CS allele or the noncancer-prone XPB/TTD allele. *Oncogene*,
736 *24*(8), 1359–1374. https://doi.org/10.1038/sj.onc.1208288
737 40. Deb, S., Xu, H., Tuynman, J. *et al.* RAD21 cohesin overexpression is a prognostic and
738 predictive marker exacerbating poor prognosis in *KRAS* mutant colorectal carcinomas. *Br*
739 *J Cancer* 110, 1606–1613 (2014). https://doi.org/10.1038/bjc.2014.3
740 41. Bordoni, M., Pansarasa, O., Dell'Orco, M., Crippa, V., Gagliardi, S., Sproviero, D.,
741 Bernuzzi, S., Diamanti, L., Ceroni, M., Tedeschi, G., Poletti, A., & Cereda, C. (2019).
742 Nuclear Phospho-SOD1 Protects DNA from Oxidative Stress Damage in Amyotrophic
743 Lateral Sclerosis. *Journal of clinical medicine*, *8*(5), 729.
744 https://doi.org/10.3390/jcm8050729
745 42. Ng, J. M., Vermeulen, W., van der Horst, G. T., Bergink, S., Sugasawa, K., Vrieling, H.,
746 & Hoeijmakers, J. H. (2003). A novel regulation mechanism of DNA repair by damage-
747 induced and RAD23-dependent stabilization of xeroderma pigmentosum group C protein.
748 *Genes & development*, *17*(13), 1630–1645. https://doi.org/10.1101/gad.260003
749 43. Brace, L. E., Vose, S. C., Stanya, K., Gathungu, R. M., Marur, V. R., Longchamp, A.,
750 Treviño-Villarreal, H., Mejia, P., Vargas, D., Inouye, K., Bronson, R. T., Lee, C. H.,
751 Neilan, E., Kristal, B. S., & Mitchell, J. R. (2016). Increased oxidative phosphorylation in
752 response to acute and chronic DNA damage. *NPJ aging and mechanisms of disease*, *2*,
753 16022. https://doi.org/10.1038/npjamd.2016.22
754 44. Nemoz, C., Ropars, V., Frit, P., Gontier, A., Drevet, P., Yu, J., Guerois, R., Pitois, A.,
755 Comte, A., Delteil, C., Barboule, N., Legrand, P., Baconnais, S., Yin, Y., Tadi, S.,
756 Barbet-Massin, E., Berger, I., Le Cam, E., Modesti, M., Rothenberg, E., … Charbonnier,
757 J. B. (2018). XLF and APLF bind Ku80 at two remote sites to ensure DNA repair by non-
758 homologous end joining. *Nature structural & molecular biology*, *25*(10), 971–980.
759 https://doi.org/10.1038/s41594-018-0133-6
760 45. Boehm, E. M., Gildenberg, M. S., & Washington, M. T. (2016). The Many Roles of
761 PCNA in Eukaryotic DNA Replication. The Enzymes, 39, 231–254.
762 https://doi.org/10.1016/bs.enz.2016.03.003
763 46. Song, M., Wang, Y., Zhang, Z., & Wang, S. (2017). PSMC2 is up-regulated in
764 osteosarcoma and regulates osteosarcoma cell proliferation, apoptosis and migration.
765 *Oncotarget*, *8*(1), 933–953. https://doi.org/10.18632/oncotarget.13511
766 47. Pujana, M. A., Han, J. D., Starita, L. M., Stevens, K. N., Tewari, M., Ahn, J. S., Rennert,
767 G., Moreno, V., Kirchhoff, T., Gold, B., Assmann, V., Elshamy, W. M., Rual, J. F.,
768 Levine, D., Rozek, L. S., Gelman, R. S., Gunsalus, K. C., Greenberg, R. A., Sobhian, B.,
769 Bertin, N., … Vidal, M. (2007). Network modeling links breast cancer susceptibility and
770 centrosome dysfunction. *Nature genetics*, *39*(11), 1338–1349.
771 https://doi.org/10.1038/ng.2007.2
772 48. Yang, S., Zhou, L., Reilly, P. T., Shen, S. M., He, P., Zhu, X. N., Li, C. X., Wang, L. S.,
773 Mak, T. W., Chen, G. Q., & Yu, Y. (2016). ANP32B deficiency impairs proliferation and
774 suppresses tumor progression by regulating AKT phosphorylation. *Cell death & disease*,
775 *7*(2), e2082. https://doi.org/10.1038/cddis.2016.8
776 49. Redza-Dutordoir, M., & Averill-Bates, D. A. (2016). Activation of apoptosis signalling
777 pathways by reactive oxygen species. *Biochimica et biophysica acta*, *1863*(12), 2977–
778 2992. https://doi.org/10.1016/j.bbamcr.2016.09.012
779 50. Rothkamm, K., & Löbrich, M. (2003). Evidence for a lack of DNA double-strand break
780 repair in human cells exposed to very low x-ray doses. *Proceedings of the National*

Academy of Sciences of the United States of America, *100*(9), 5057–5062. https://doi.org/10.1073/pnas.0830918100

51. Marín, A., Martín, M., Liñán, O., Alvarenga, F., López, M., Fernández, L., Büchser, D., & Cerezo, L. (2014). Bystander effects and radiotherapy. *Reports of practical oncology and radiotherapy : journal of Greatpoland Cancer Center in Poznan and Polish Society of Radiation Oncology*, *20*(1), 12–21. https://doi.org/10.1016/j.rpor.2014.08.004
52. Cadet, J., & Wagner, J. R. (2013). DNA base damage by reactive oxygen species, oxidizing agents, and UV radiation. *Cold Spring Harbor perspectives in biology*, *5*(2), a012559. https://doi.org/10.1101/cshperspect.a012559
53. Kennedy A. R. (2014). Biological Effects of Space Radiation and Development of Effective Countermeasures. *Life sciences in space research*, *1*, 10–43. https://doi.org/10.1016/j.lssr.2014.02.004
54. Thannickal, V. J., & Fanburg, B. L. (2000). Reactive oxygen species in cell signaling. *American journal of physiology. Lung cellular and molecular physiology*, *279*(6), L1005–L1028. https://doi.org/10.1152/ajplung.2000.279.6.L1005
55. Stier, A., Schull, Q., Bize, P. *et al.* Oxidative stress and mitochondrial responses to stress exposure suggest that king penguins are naturally equipped to resist stress. *Sci Rep* 9, 8545 (2019). https://doi.org/10.1038/s41598-019-44990-x
56. Ock, C. Y., Kim, E. H., Choi, D. J., Lee, H. J., Hahm, K. B., & Chung, M. H. (2012). 8-Hydroxydeoxyguanosine: not mere biomarker for oxidative stress, but remedy for oxidative stress-implicated gastrointestinal diseases. *World journal of gastroenterology*, *18*(4), 302–308. https://doi.org/10.3748/wjg.v18.i4.302
57. Lee, S. H., Meng, X. W., Flatten, K. S., Loegering, D. A., & Kaufmann, S. H. (2013). Phosphatidylserine exposure during apoptosis reflects bidirectional trafficking between plasma membrane and cytoplasm. *Cell death and differentiation*, *20*(1), 64–76. https://doi.org/10.1038/cdd.2012.93
58. Wang, S., El-Deiry, W. TRAIL and apoptosis induction by TNF-family death receptors. *Oncogene* 22, 8628–8633 (2003). https://doi.org/10.1038/sj.onc.1207232
59. Duez, P., Dehon, G., Kumps, A., & Dubois, J. (2003). Statistics of the Comet assay: a key to discriminate between genotoxic effects. *Mutagenesis*, *18*(2), 159–166. https://doi.org/10.1093/mutage/18.2.159
60. Elmore S. (2007). Apoptosis: a review of programmed cell death. *Toxicologic pathology*, *35*(4), 495–516. https://doi.org/10.1080/01926230701320337
61. Bowden, R. D., Buckwalter, M. R., McBride, J. F., Johnson, D. A., Murray, B. K., & O'Neill, K. L. (2003). Tail profile: a more accurate system for analyzing DNA damage using the Comet assay. *Mutation research*, *537*(1), 1–9. https://doi.org/10.1016/s1383-5718(03)00056-1
62. Collins, A. R., Dobson, V. L., Dusinská, M., Kennedy, G., & Stětina, R. (1997). The comet assay: what can it really tell us?. *Mutation research*, *375*(2), 183–193. https://doi.org/10.1016/s0027-5107(97)00013-4
63. Mair, P., Wilcox, R. Robust statistical methods in R using the WRS2 package. *Behav Res* **52,** 464–488 (2020). https://doi.org/10.3758/s13428-019-01246-w
64. Korotkevich G, Sukhov V, Sergushichev A (2019). "Fast gene set enrichment analysis." *bioRxiv*. doi: 10.1101/060012, http://biorxiv.org/content/early/2016/06/20/060012.

65. Lin, Y., Boone, M., Meuris, L. *et al.* Genome dynamics of the human embryonic kidney 293 lineage in response to cell biology manipulations. *Nat Commun* **5,** 4767 (2014). https://doi.org/10.1038/ncomms5767
66. Purbey, P. K., Scumpia, P. O., Kim, P. J., Tong, A. J., Iwamoto, K. S., McBride, W. H., & Smale, S. T. (2017). Defined Sensing Mechanisms and Signaling Pathways Contribute to the Global Inflammatory Gene Expression Output Elicited by Ionizing Radiation. *Immunity*, *47*(3), 421–434.e3. https://doi.org/10.1016/j.immuni.2017.08.017
67. Ma, H., Rao, L., Wang, H. *et al.* Transcriptome analysis of glioma cells for the dynamic response to γ-irradiation and dual regulation of apoptosis genes: a new insight into radiotherapy for glioblastomas. *Cell Death Dis* **4,** e895 (2013). https://doi.org/10.1038/cddis.2013.412
68. Hurov, K. E., Cotta-Ramusino, C., & Elledge, S. J. (2010). A genetic screen identifies the Triple T complex required for DNA damage signaling and ATM and ATR stability. *Genes & development*, *24*(17), 1939–1950. https://doi.org/10.1101/gad.1934210
69. Samuni, A. M., Kasid, U., Chuang, E. Y., Suy, S., Degraff, W., Krishna, M. C., Russo, A., & Mitchell, J. B. (2005). Effects of hypoxia on radiation-responsive stress-activated protein kinase, p53, and caspase 3 signals in TK6 human lymphoblastoid cells. *Cancer research*, *65*(2), 579–586.
70. Wang, H., Jiang, H., Van De Gucht, M., & De Ridder, M. (2019). Hypoxic Radioresistance: Can ROS Be the Key to Overcome It?. *Cancers*, *11*(1), 112. https://doi.org/10.3390/cancers11010112
71. Contiliani, D. F., de Araújo Ribeiro, Y., de Moraes, V. N., & Pereira, T. C. (2020). *Panagrolaimus superbus* tolerates hypoxia within Gallium metal cage: implications for the understanding of the phenomenon of anhydrobiosis. *Journal of nematology*, *52*, 1–6. https://doi.org/10.21307/jofnem-2020-046
72. Wang, C., Grohme, M. A., Mali, B., Schill, R. O., & Frohme, M. (2014). Towards decrypting cryptobiosis--analyzing anhydrobiosis in the tardigrade Milnesium tardigradum using transcriptome sequencing. *PloS one*, *9*(3), e92663. https://doi.org/10.1371/journal.pone.0092663
73. Vilas, C. K., Emery, L. E., Denchi, E. L., & Miller, K. M. (2018). Caught with One's Zinc Fingers in the Genome Integrity Cookie Jar. *Trends in genetics : TIG*, *34*(4), 313–325. https://doi.org/10.1016/j.tig.2017.12.011
74. Chen, E. Y., Tan, C. M., Kou, Y., Duan, Q., Wang, Z., Meirelles, G. V., Clark, N. R., & Ma'ayan, A. (2013). Enrichr: interactive and collaborative HTML5 gene list enrichment analysis tool. *BMC bioinformatics*, *14*, 128. https://doi.org/10.1186/1471-2105-14-128
75. Kuleshov, M. V., Jones, M. R., Rouillard, A. D., Fernandez, N. F., Duan, Q., Wang, Z., Koplev, S., Jenkins, S. L., Jagodnik, K. M., Lachmann, A., McDermott, M. G., Monteiro, C. D., Gundersen, G. W., & Ma'ayan, A. (2016). Enrichr: a comprehensive gene set enrichment analysis web server 2016 update. *Nucleic acids research*, *44*(W1), W90–W97. https://doi.org/10.1093/nar/gkw377
76. Dobin, A., Davis, C. A., Schlesinger, F., Drenkow, J., Zaleski, C., Jha, S., Batut, P., Chaisson, M., & Gingeras, T. R. (2013). STAR: ultrafast universal RNA-seq aligner. *Bioinformatics (Oxford, England)*, *29*(1), 15–21. https://doi.org/10.1093/bioinformatics/bts635
77. Conesa, A., Madrigal, P., Tarazona, S., Gomez-Cabrero, D., Cervera, A., McPherson, A., Szcześniak, M. W., Gaffney, D. J., Elo, L. L., Zhang, X., & Mortazavi, A. (2016). A

survey of best practices for RNA-seq data analysis. *Genome biology*, *17*, 13. https://doi.org/10.1186/s13059-016-0881-8

78. Li, H., Handsaker, B., Wysoker, A., Fennell, T., Ruan, J., Homer, N., Marth, G., Abecasis, G., Durbin, R., & 1000 Genome Project Data Processing Subgroup (2009). The Sequence Alignment/Map format and SAMtools. *Bioinformatics (Oxford, England)*, *25*(16), 2078–2079.
79. Love, M.I., Huber, W. & Anders, S. Moderated estimation of fold change and dispersion for RNA-seq data with DESeq2. *Genome Biol* **15,** 550 (2014). https://doi.org/10.1186/s13059-014-0550-8
80. Liberzon, A., Birger, C., Thorvaldsdóttir, H., Ghandi, M., Mesirov, J. P., & Tamayo, P. (2015). The Molecular Signatures Database (MSigDB) hallmark gene set collection. *Cell systems*, *1*(6), 417–425. https://doi.org/10.1016/j.cels.2015.12.004
81. Subramanian, A., Tamayo, P., Mootha, V. K., Mukherjee, S., Ebert, B. L., Gillette, M. A., Paulovich, A., Pomeroy, S. L., Golub, T. R., Lander, E. S., & Mesirov, J. P. (2005). Gene set enrichment analysis: a knowledge-based approach for interpreting genome-wide expression profiles. *Proceedings of the National Academy of Sciences of the United States of America*, *102*(43), 15545–15550. https://doi.org/10.1073/pnas.0506580102
82. Liao, Y., Wang, J., Jaehnig, E. J., Shi, Z., & Zhang, B. (2019). WebGestalt 2019: gene set analysis toolkit with revamped UIs and APIs. *Nucleic acids research*, *47*(W1), W199–W205. https://doi.org/10.1093/nar/gkz401
83. Zhang, B., Kirov, S., & Snoddy, J. (2005). WebGestalt: an integrated system for exploring gene sets in various biological contexts. *Nucleic acids research*, *33*(Web Server issue), W741–W748. https://doi.org/10.1093/nar/gki475
84. Schmidt, M. A., Meydan, C., Schmidt, C. M., Afshinnekoo, E., & Mason, C. E. (2020). The NASA Twins Study: The Effect of One Year in Space on Long-Chain Fatty Acid Desaturases and Elongases. *Lifestyle genomics*, *13*(3), 107–121. https://doi.org/10.1159/000506769
85. MacKay M, Afshinnekoo E, Roboz G, Guzman M, Melnick A, Wu S, Mason CE. The Therapeutic Landscape for Cells Engineered with Chimeric Antigen Receptors. *Nature Biotechnology*. 2020 Jan;6(8):120-128.

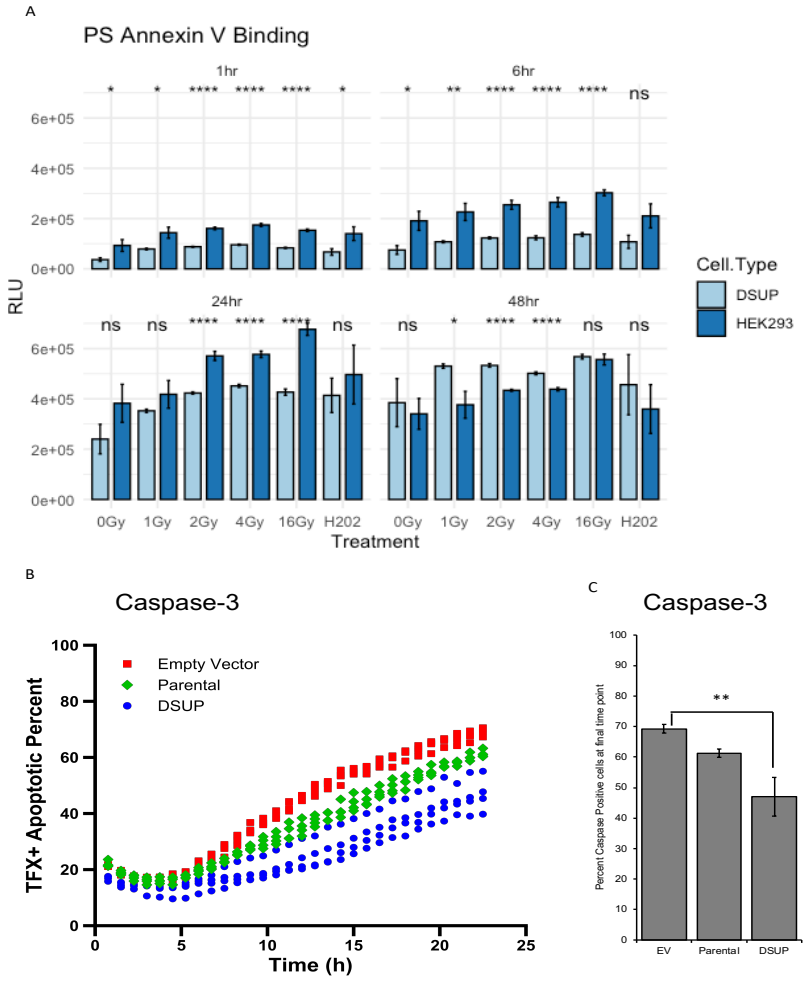

Figure 1. Apoptosis Assay.

A) Apoptosis was measured by Phosphatidyl Serine exposure to luminescent annexin V fusion proteins (Annexin V-LgBit and Annexin VsmBit). HEK293 Dsup and HEK293 controls were subjected to 1Gy, 2Gy, 4Gy, and 16Gy of X-ray radiation and 100µM of H202 for the duration of the time points 1hr, 6hr, 24hrs, and 48hrs. At each time point apoptosis was measured in terms of relative light units (RLUs). HEK293 control cells experience roughly twice as much apoptotic signals than HEK293 DSUP up to 24hrs but then saturates at 48hrs. Anova analysis followed by Tukeys Post Hoc test was used to determine p value significance, ns=p>0.05, p=0.5*, ** p<0.05, *** p<0.01, **** p<0.001. Values represent average of triplicates and error bars represent standard error of the mean.

B) Apoptosis via caspase-3 activity was measured in HEK293, Empty vector, and Dsup expressing cells. 13.2uM of CPT was added to each cell line and Hoechst and Caspase staining was used to discriminate live cells from apoptotic cells. Images were collected and FITC intensity was analyzed and plotted over time for all wells.

C) Percentage of apoptotic cells at the end of the experiment was calculated at 22.5 hours. Error bars show 1 standard deviation of the apoptotic rate of the cells. A heteroscedastic two tailed student t-test was used to test the null hypothesis that the empty vector and Dsup containing cells have equal rates of apoptosis (p = 0.005).

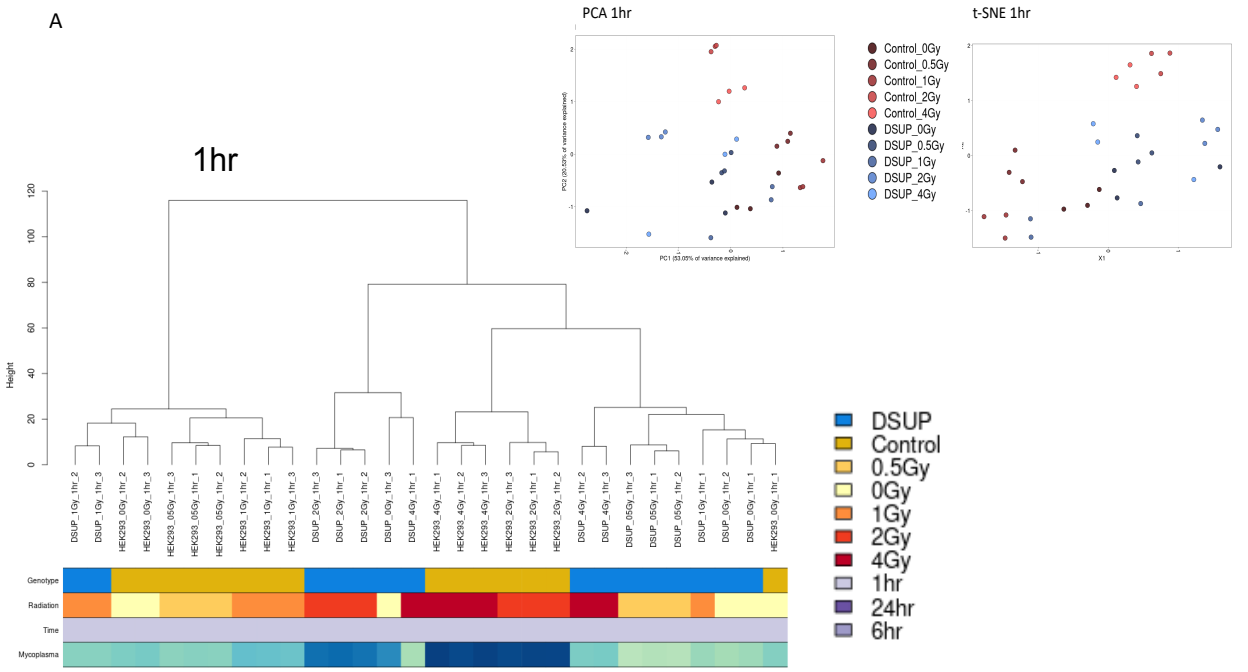
A
1hr
PCA 1hr
t-SNE 1hr
Control_0Gy
Control_0.5Gy
Control_1Gy
Control_2Gy
Control_4Gy
DSUP_0Gy
DSUP_0.5Gy
DSUP_1Gy
DSUP_2Gy
DSUP_4Gy
Height
Genotype
Radiation
Time
Mycoplasma
DSUP
Control
0.5Gy
0Gy
1Gy
2Gy
4Gy
1hr
24hr
6hr

925

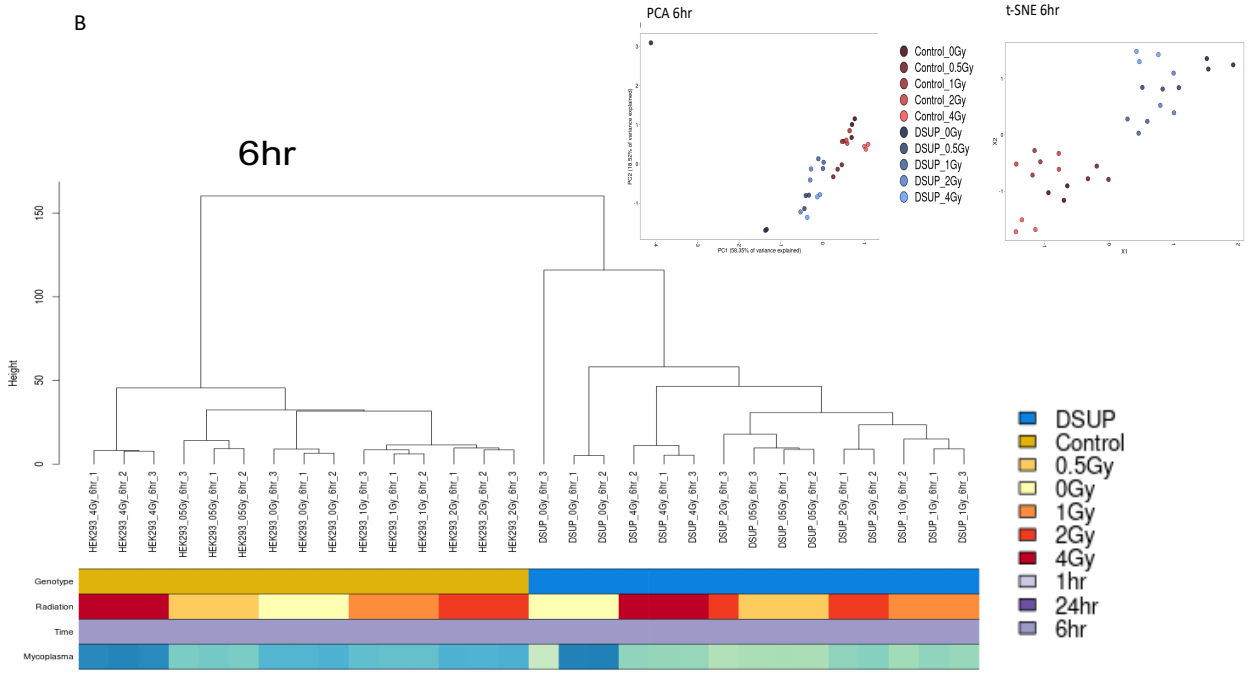
B
6hr
PCA 6hr
t-SNE 6hr
Control_0Gy
Control_0.5Gy
Control_1Gy
Control_2Gy
Control_4Gy
DSUP_0Gy
DSUP_0.5Gy
DSUP_1Gy
DSUP_2Gy
DSUP_4Gy
Height
Genotype
Radiation
Time
Mycoplasma
DSUP
Control
0.5Gy
0Gy
1Gy
2Gy
4Gy
1hr
24hr
6hr

926

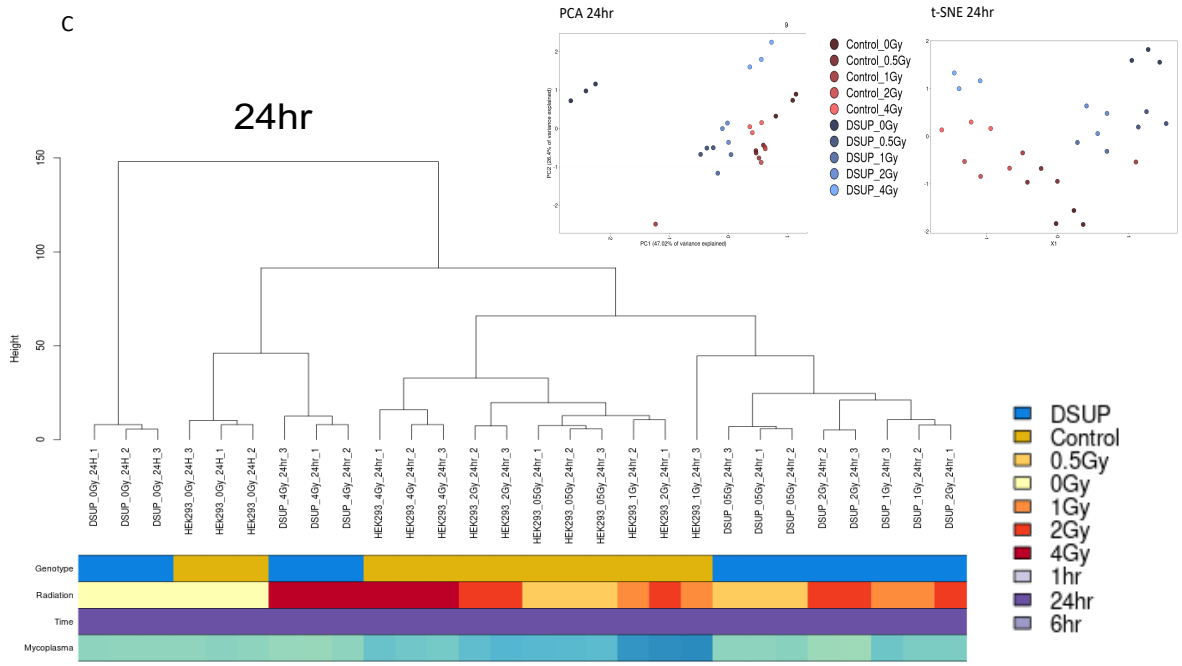

Figure 2. Clustering reveals separation of time and genotype.
A) Pearson correlated hierarchical clustering of gene expression, principal component analysis (PCA), and T-distributed Stochastic Neighbor Embedding (t-SNE) dimensionality reduction techniques for 1hr post radiation B) Pearson correlated hierarchical clustering of gene expression, principal component analysis (PCA), and T-distributed Stochastic Neighbor Embedding (t-SNE) dimensionality reduction techniques for 6hrs post radiation C) Pearson correlated hierarchical clustering of gene expression, principal component analysis (PCA), and T-distributed Stochastic Neighbor Embedding (t-SNE) dimensionality reduction techniques for 24hrs post radiation shows different clustering of HEK293 DSUP vs HEK293. Clustering of all time points reveals high variance clustering of HEK293 Dsup at 6hr and 24hrs at 0Gy baseline. Clear groupings between HEK293 Dsup and Controls can be seen at individual hours. PCA and t-SNE analysis reveals that clustering is more based on time and genotype rather than dose.

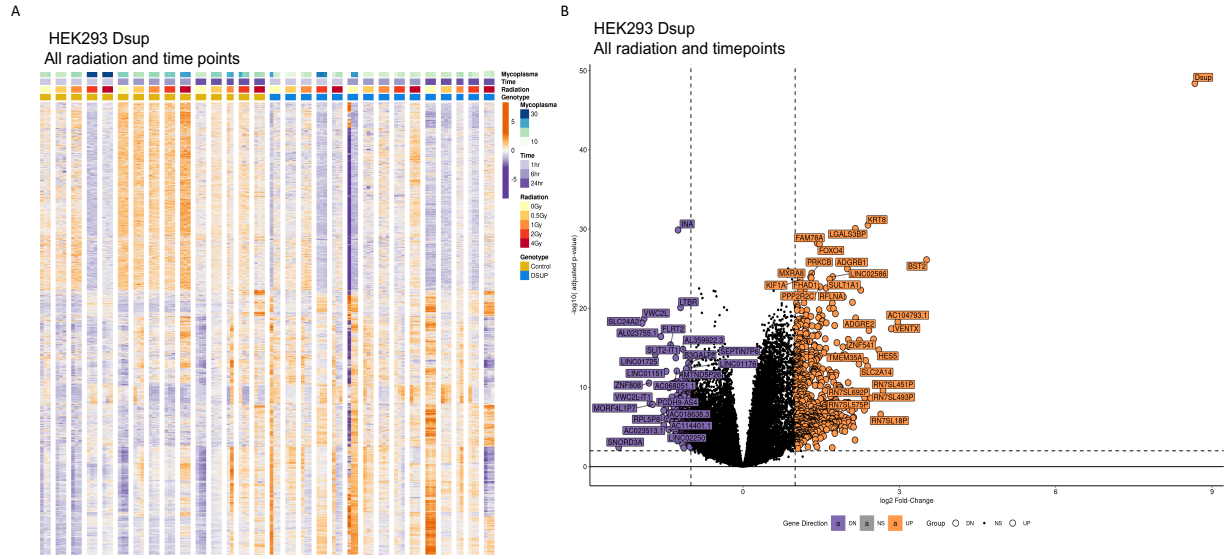

Figure 3. HEK293 Dsup response to radiation and time.

A) Heatmap for HEK293 and Dsup cells across all radiation doses and time points. Gene expression changes were seen across each time point and mostly corresponded to time and genotype. Reported here are genes expression changes for any gene with a $q<0.01$ and $logFC \geq 1$ in a multivariate model including mycoplasma correction, time, radiation, and genotype. Orange indicates relative enrichment while purple indicates relative depletion. Differences in gene clustering at 0Gys across all time points indicates gene expression differences for Dsup expressing cells at baseline.

B) Volcano plot illustrating fold change log base 2 compared with adjusted p value (-log base 10) between HEK293 Dsup and HEK293 controls across all time points. Horizontal bar at y=2 represents a significance level of $p = 0.01$ significance level. Dsup is the most differentially and significantly expressed gene across all time points.

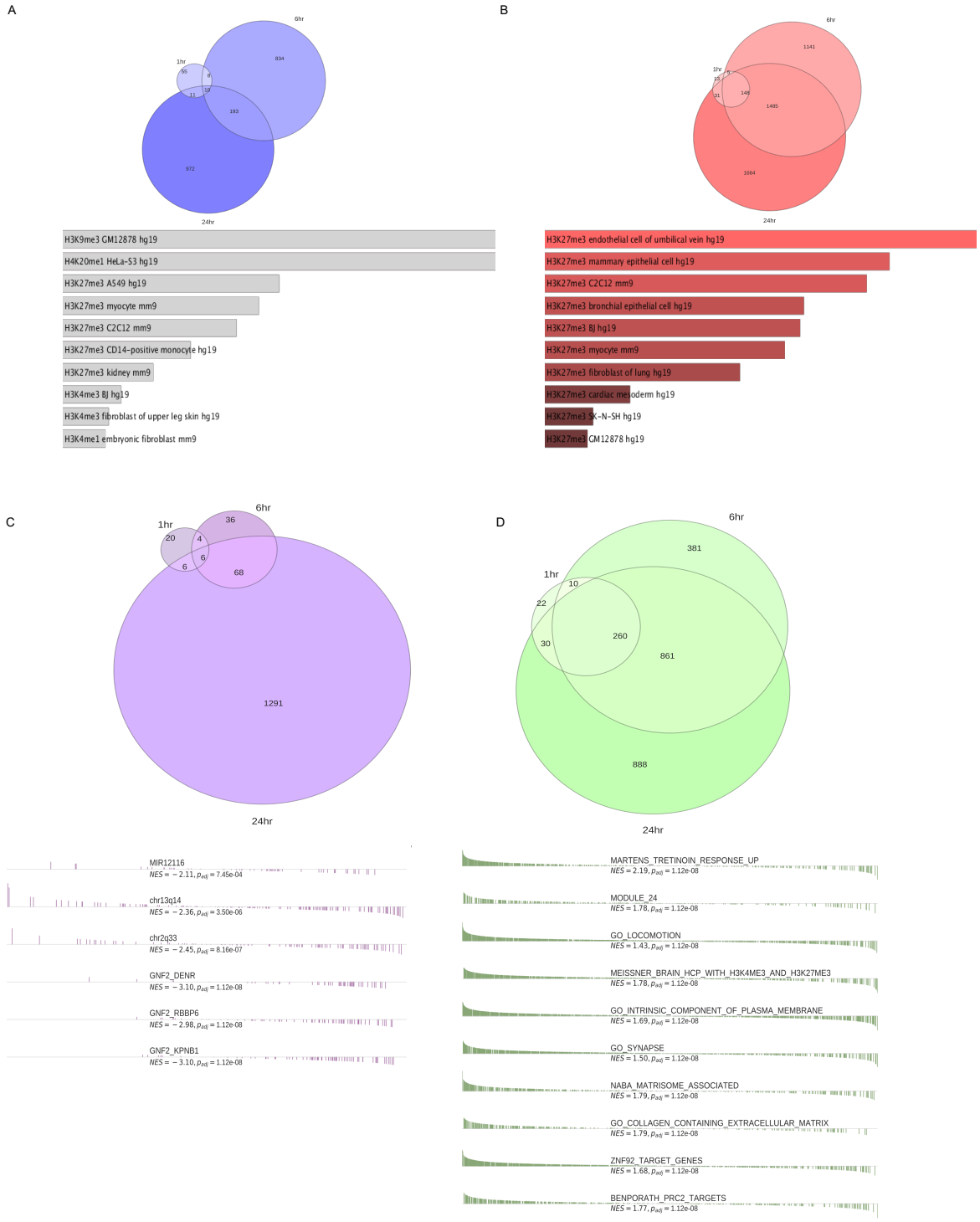

Figure 4. Shared pathways conserved across 0Gys at all timepoints.
ENCODE histone modifications were assessed using Enrichr with bars sorted by p-value rankings
A) The 10 genes that were found downregulated across all time points histone modification pathways were analyzed. Gray bars are not significantly expressed and the top corresponding bar has a q-value of 1
B) The subset of the intersection of all genes upregulated at 0Gys was 148 genes and was analyzed for histone modification pathways. Red bars indicate significantly expressed histone methylation pathways with the top bar having an associated q-value of 7.941e-11.

C) Fgsea Running Enrichment Score plots corresponding to each time point at all doses of radiation for downregulated pathways in Dsup expressing cells. Horizontal lines correspond to ranked leading edge subset. Fgsea plots are ordered by p-adjusted values and correlated with density of genes of the curve.
D) Upregulated pathways across all time points for all doses of radiation.

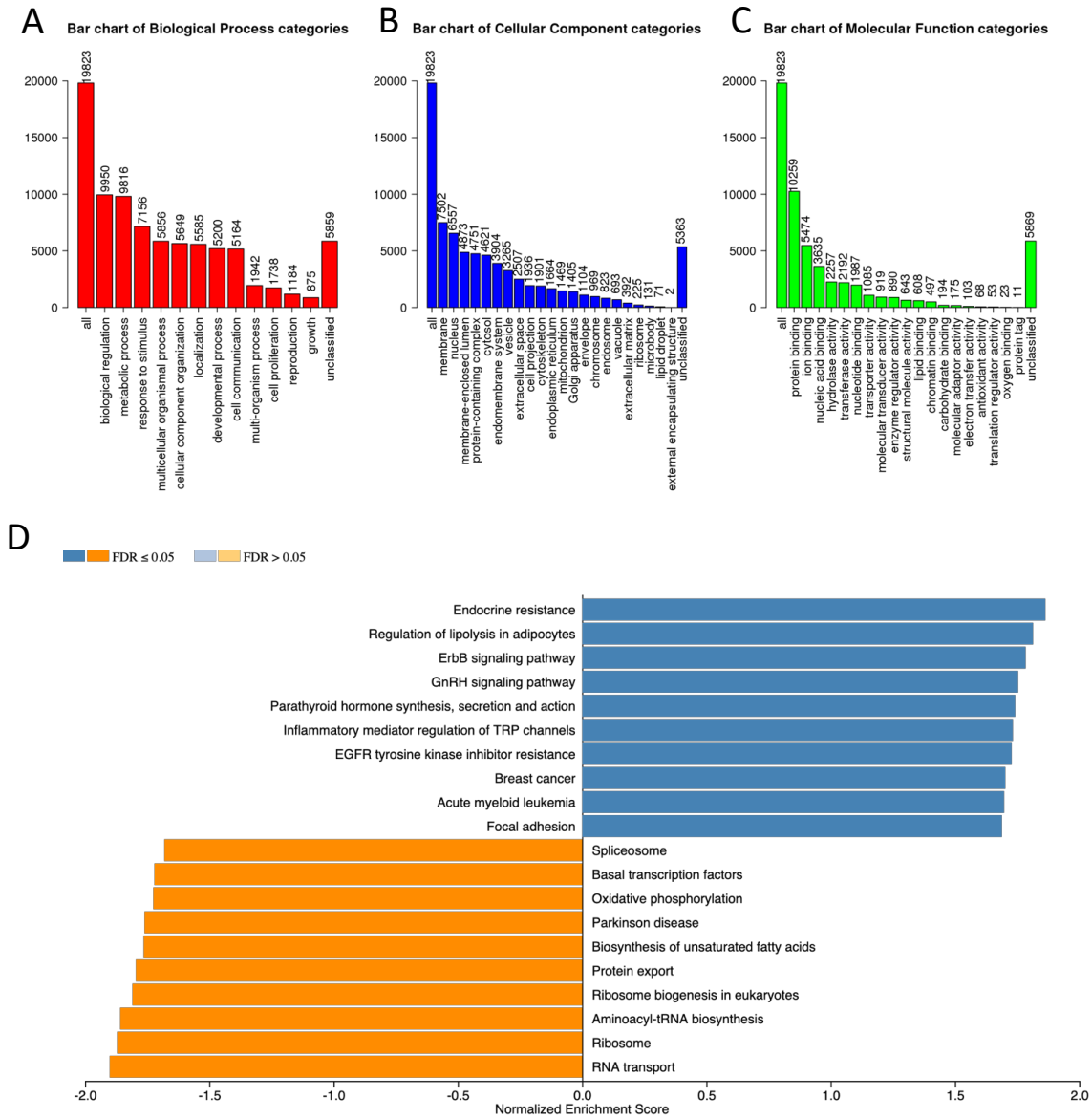

Figure 5. Functional GSEA of Kegg pathways.
Genes were ranked by a p-value cutoff of .05 and Log_2FC cutoff of 1.5 was used to perform WebGesalt GSEA for overall comparison of differentially expressed pathways in HEK293 Dsup vs. HEK293.
A) Biological process shows top enrichment of biological regulation, metabolic process, and response to stimulus.
B) Cellular component shows top enrichment of membrane, nucleus, and membrane enclosed lumen
C) Molecular function shows top enrichment of protein binding, ion binding, and nucleic acid binding.
D) Enrichment ratio**.** Displays top upregulated and top downregulated KEGG pathways for Dsup expressing human cells compared to WT.

Supplemental Figures

A

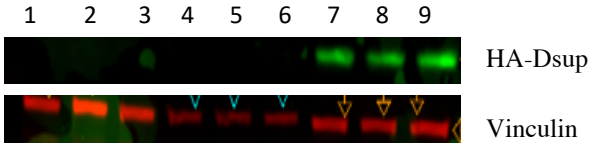

B

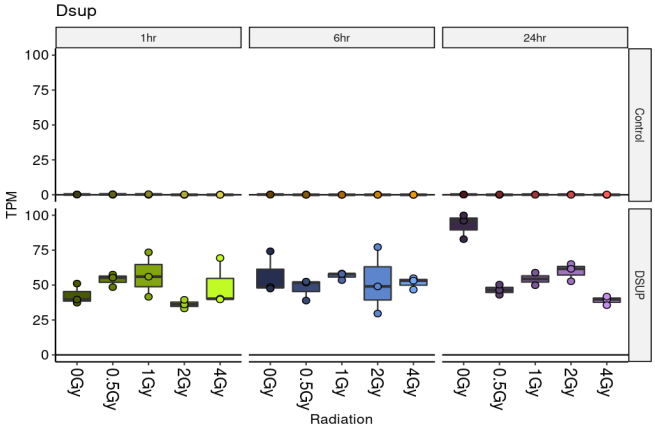

Figure S1. Presence of HA-tagged DSUP.

A) Primary antibodies R&D Systems recombinant mouse HA Tag antibody (MAB0601) was diluted to 0.1ug/ml and Anti Human Vinculin antibody (V284) was diluted to a working concentration of 1:500 dilution and used as a housekeeping protein control. Invitrogen Goat anti-Rabbit IgG (H+L) Cross-Absorbed Secondary Antibody DyLight 800 (SAS-10036) and Rabbit anti-Mouse IgG (H+L) Cross-adsorbed Secondary Antibody Alexa Fluor Plus 680 (A32729) diluted to working concentrations of 1:5000 dilution and 0.1ug/ml respectively in 1% milk in 1X TBST. The blot was imaged on a Li-Cor Odyssey® CLx imagine system using both 700nm and 800nm channels. Viniculin was present in all samples at 110kDa and only HA tag at 43 kDa indicative of the MW of Dsup. Columns 1-3 are HEK293, 4-6 are HEK293 Vector, and 7-9 are HEK293-Dsup expressing HA tag.

B) Boxplots shows presence of Dsup transcripts in HEK293-Dsup cells but not in control across all time points and doses of radiation.

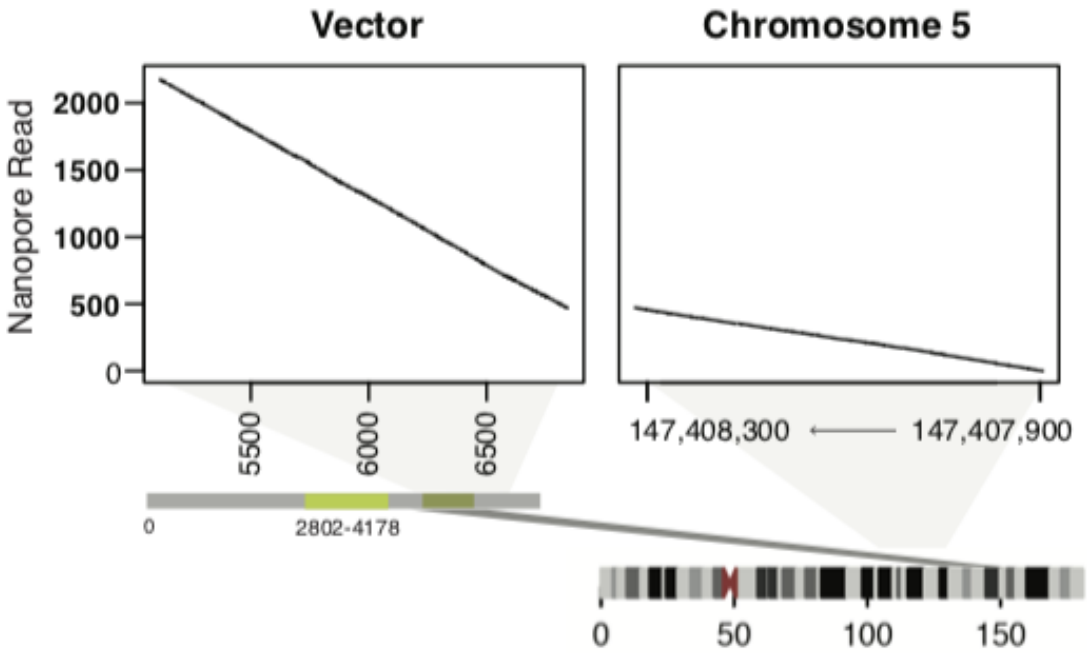

991
992 **Figure S2. Identification of insertion site.**
993 The left plot x-axis is the segment of the read that maps to the vector and the right plot x-axis is the segment of the
994 read that maps to the genome. The y-axis is the full length nanopore read. The first 500 bases of the nanopore read
995 map to the right arm of chromosome 5 while the remaining 1500 bases of the nanopore read map to the vector site
996 downstream of Dsup. 98% of reads were obtained for HEK293 parental cell line and HEK293 Dsup with a genome
997 coverage of ~2.8x and 1.1x respectively.
998
999
1000

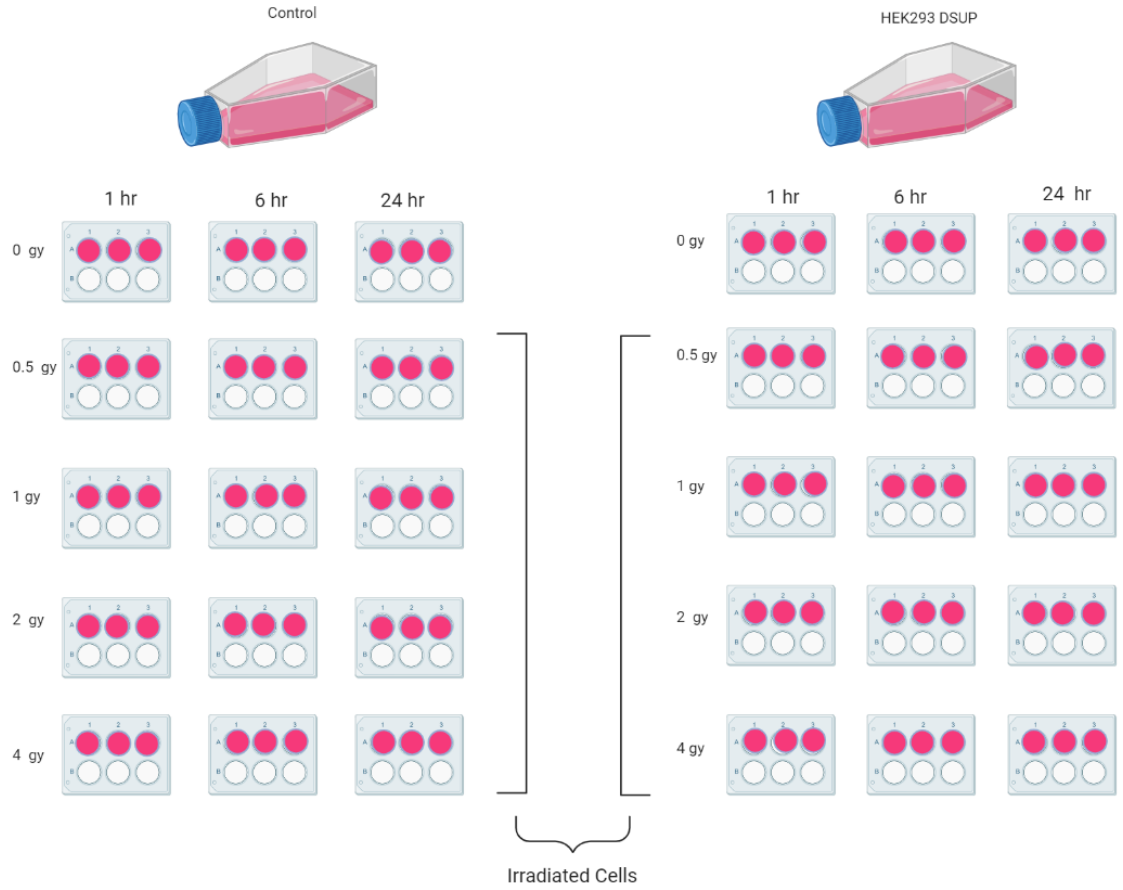

Figure S3. Experimental layout for RNAseq analysis.
HEK293 Dsup and Control cells were grown to 75% confluency on T-175 flasks before plated in triplicates on 6 well plates. 1 day after seeding, cells from each set were irradiated with X-rays in a RS2000 Biological research irradiator. For 0Gy, each set was kept outside the incubator at the corresponding time frame it took to irradiate cells and were harvested along with irradiated cells at 1hr, 6hrs, and 24hrs, post irradiation.

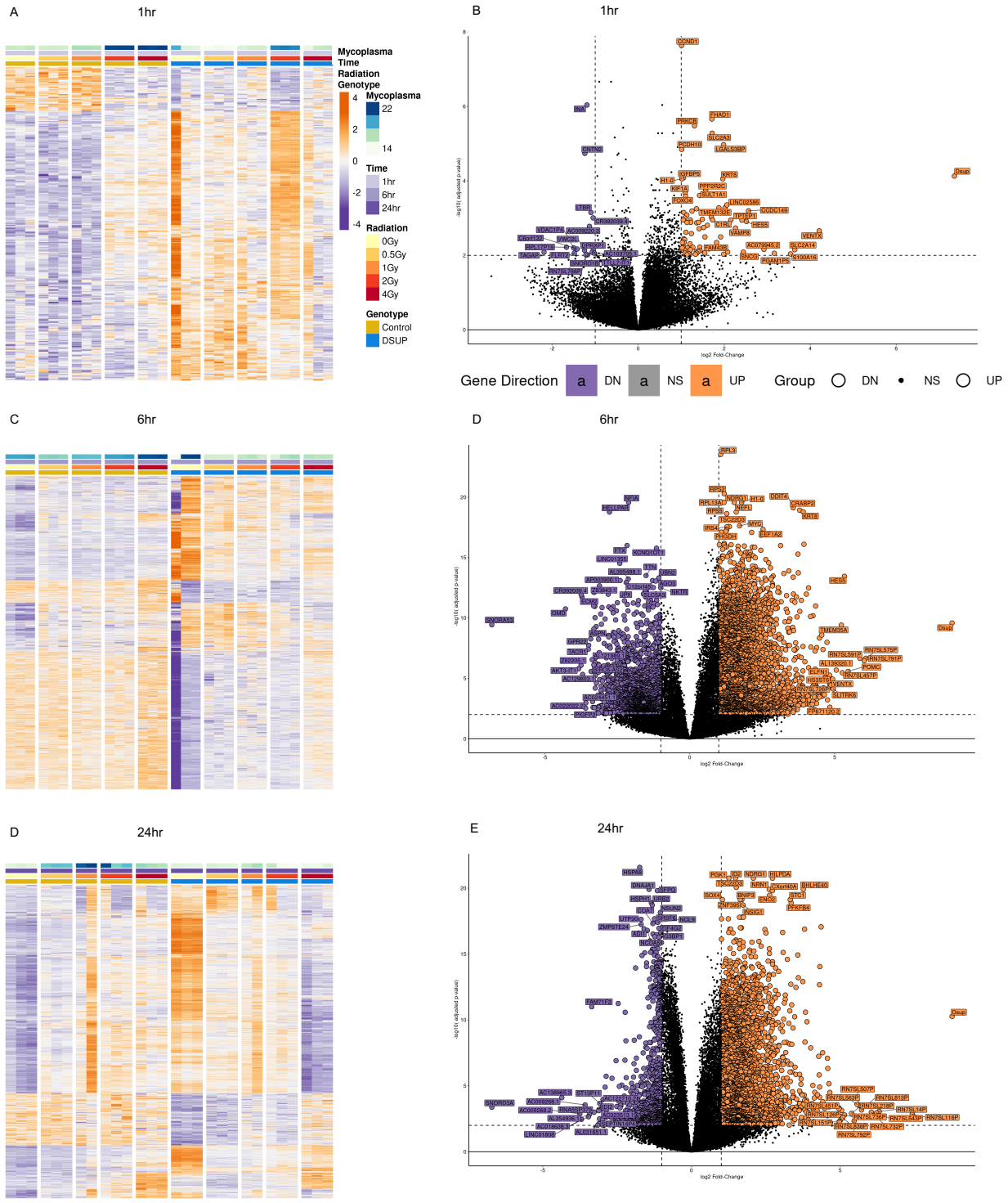

Figure S4. A) Heatmap for mycoplasma corrected HEK293 and DSUP cell lines across all radiation doses at 1hr post radiation.
B) Volcano plot illustrating mycoplasma corrected gene fold change log base 2 compared with adjusted p value (-log base 10) between HEK293 DSUP and HEK293 controls across all radiation doses at 1hr post radiation.
C) Heatmap for mycoplasma corrected HEK293 and DSUP cell lines across all radiation doses at 6hr post radiation.
D) Volcano plot illustrating mycoplasma corrected gene fold change log base 2 compared with adjusted p value (-log base 10) between HEK293 DSUP and HEK293 controls across all radiation doses at 6hr post radiation.

E) Heatmap for mycoplasma corrected HEK293 and DSUP cell lines across all radiation doses at 24hr post radiation.
F) Volcano plot illustrating mycoplasma corrected gene fold change log base 2 compared with adjusted p value (-log base 10) between HEK293 DSUP and HEK293 controls across all radiation doses at 24hr post radiation.

A

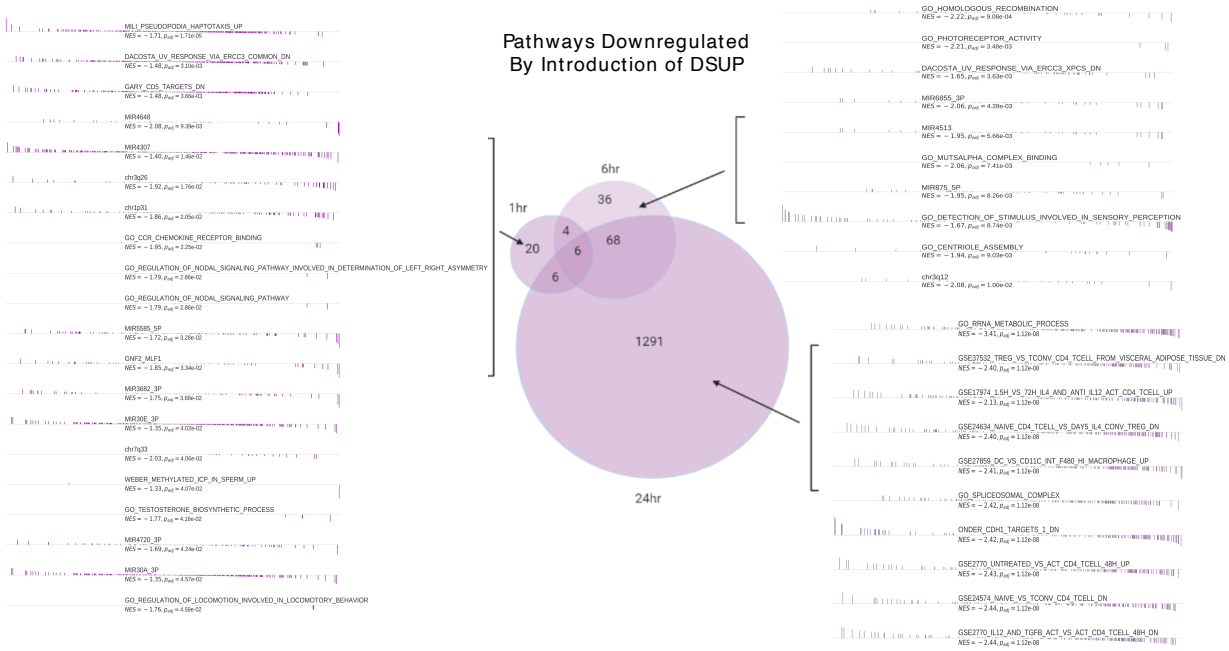

B

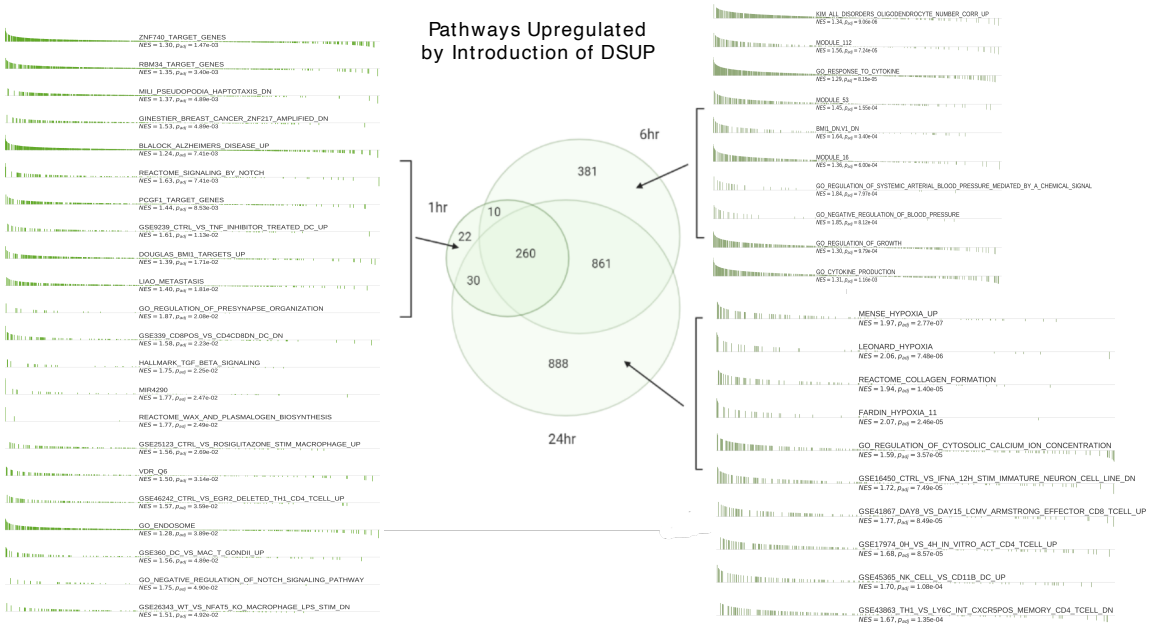

Figure S5. Differentially expressed pathways by introduction of Dsup at each timepoint.

(A) Fgsea Running Enrichment Score plots corresponding to each time point at all doses of radiation for downregulated pathways in Dsup expressing cells. Horizontal lines correspond to ranked leading edge subset. Fgsea plots are ordered by p.adjusted values and correlated with density of genes of the curve.
(B) Upregulated pathways across all time points for all doses of radiation.

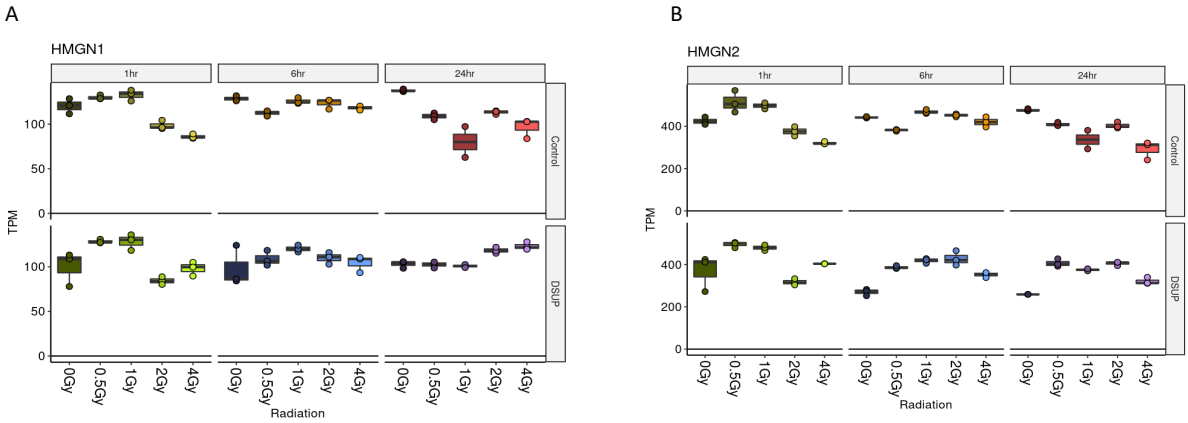

Figure S6. Stable expression of HMGN1/2. Fgsea Boxplots of TPM normalized gene expression of human homologous proteins HMGN1 and HMGN2 reveal relatively normal expression across time points for both HEK293 Dsup and HEK293 control cells.